ANL/LWRS-22/2

Effect of thermal aging on microstructure and crack growth response of Alloy 152 Weld

LWRS milestone Report Number: M3LW-22OR0402035

Nuclear Science and Engineering Division
Argonne National Laboratory

ANL/LWRS-22/2

Effect of thermal aging on microstructure and crack growth response of Alloy 152 Weld

LWRS milestone Report Number: M3LW-22OR0402035

Bogdan Alexandreanu, Yiren Chen, Xuan Zhang and Wei-Ying Chen

Nuclear Science and Engineering Division, Argonne National Laboratory

September 2022

This page intentionally left blank

ABSTRACT

Nickel-based Alloy 690 and the associated weld Alloys 52 and 152 are typically used for nozzle penetrations in replacement heads for pressurized water reactor (PWR) vessels, because of their excellent overall resistance to general corrosion and environmental degradation, primarily stress corrosion cracking (SCC). However, many of the existing PWRs are expected to operate for 40-80 years. Likewise, advanced water-cooled small modular reactors (SMRs) will use Ni-Cr alloys and are expected to receive initial operating licenses for 60 years. Hence, the thermal stability of Ni-Cr alloys is a potential concern for the long-term performance of both existing and advanced nuclear power plants, and possibly spent fuel storage containers. The objective of this research is to understand the microstructural changes occurring in high-Cr, Ni-based Alloy 152 weldments during long time exposure to the reactor operating temperatures, and the effect of these changes on the service performance. One area of particular concern is the potential for long range ordering (LRO), *i.e.* formation of the intermetallic Ni_2Cr phase under prolonged exposure to reactor temperatures and/or irradiation, which can increase strength, decrease ductility, and cause dimensional changes or lead to in-service embrittlement of components made with these alloys. Hence, this research focused on the microstructural evolution and the SCC response of Alloy 152 under accelerated thermal aging. The materials studied involved three heats of Alloy 152 used to produce a dissimilar metal weld (DMW) joining an Alloy 690 plate to an Alloy 533 low alloy steel (LAS) plate, thermally aged at three different temperatures (370°C, 400°C and 450°C) for up to 75,000h (equivalent to 60 years of service). The microstructural characterization by means of synchrotron X-ray did not find evidence of LRO in any of the three heats aged to an equivalent of 60 years of service. Testing in a primary water environment of a heat of Alloy 152 aged at 370°C to a 60-year service equivalent revealed a fatigue and corrosion fatigue crack growth responses similar to those measured on the un-aged alloy. However, the SCC CGR response of the aged sample appears to show a deterioration in performance.

TABLE OF CONTENTS

LIST OF FIGURES

LIST OF TABLES

ABBREVIATIONS

ANL	Argonne National Laboratory
APS	Advanced Photon Source
ASTM	American Society for Testing and Materials
BPR	Back Pressure Regulator
BWR	Boiling Water Reactor
CGR	Crack Growth Rate
CL	Constant Load
CMTR	Certified Material Test Report
CSL	Coincident Site Lattice
CT	Compact Tension
DO	Dissolved Oxygen
DMW	Dissimilar Metal Weld
ECP	Electrochemical Potential
EDX	Energy Dispersive X-ray Spectroscopy
EPRI MRP	Electric Power Research Institute Materials Reliability Program
GBE	Grain Boundary Engineering
GTAW	Gas Tungsten Arc Welding
HAZ	Heat Affected Zone
HX	Heat Exchanger
IG	Intergranular
LAS	Low Alloy Steel
LWR	Light Water Reactor
NRC	Nuclear Regulatory Commission
PPU	Partial Periodic Unloading
PWR	Pressurized Water Reactor
PWHT	Post Weld Heat Treatment
PWSCC	Primary Water Stress Corrosion Cracking
SCC	Stress Corrosion Cracking
SEM	Scanning Electron Microscopy
SMAW	Shielded Metal Arc Welding
SS	Stainless Steel
S	Side
T	Transverse
TC	Thermocouple
TG	Transgranular
WOL	Weld Overlay
WPS	Weld Procedure Specification

ACKNOWLEDGMENTS

This research was supported through the U.S. Department of Energy's Light Water Reactor Sustainability program, Materials Research Pathway. Program managers: Dr. Thomas. M. Rosseel and Dr. Xiang (Frank) Chen.

1 Introduction

Nickel-based Alloy 690 and the associated weld Alloys 52 and 152 are typically used for nozzle penetrations in replacement heads for pressurized water reactor (PWR) vessels, because of their increased resistance to stress corrosion cracking (SCC) relative to Alloys 600, 82, and 182 [1, 2]. Many of these reactors are expected to operate for 40-80 years. Likewise, advanced water-cooled small modular reactors (SMRs) will use Ni-Cr alloys in their primary systems and are expected to receive initial operating licenses for 60 years. For spent fuel containers, the desired lifetime is 10,000 years. Hence, the thermal stability of Ni-Cr alloys is a potential concern for the long-term performance of nuclear plants and possibly spent fuel storage containers.

One area of concern is that the long time exposure to reactor operating temperatures can result in long range ordering (LRO), *i.e.* formation of the intermetallic Ni_2Cr phase which can lead to in-service embrittlement of Ni-Cr components. Research with binary Ni-Cr binary alloys by Young et al [3] have found that LRO promotes SCC, with an SCC CGR 1,000x larger than the non-ordered version of the alloy. However, Fe plays a key role in the development of LRO, and it is not clear at this time whether LRO occurs in commercial heats as the addition of Fe was found to hinder LRO formation [4].

Perhaps the most comprehensive study on LRO of Alloy 690 was conducted by Framatome/ EdF [5, 6]. One of the main findings of this study was that an Alloy 690 heat with 7.2 wt. % Fe requires 70,000 h to develop LRO at 420°C, while ordering had not occurred in Alloy 690 with 10.4 wt. % Fe aged for 70,000 h at the same temperature. 20% added cold-work was found to decrease the time to develop LRO slightly, to 60,000h. More recently, Huotilainen et al. found significant increases in hardness in two of the four heats aged up to 10,000h at 400°C [7]. The two heats that hardened had a lower Fe content than the heats that did not harden as a result of aging (9.53 and 9.3 wt. % vs. 10.37 and 10.04 wt. %). The latter observation is consistent with the formation of LRO as its kinetics is known to decrease with the increase of Fe concentration, however, Fe levels of up to 10 wt. % were found not to impede the LRO formation [4]. Nevertheless, the hardening reported in two of the four heats is similar to that resulting from 15-20% added cold work [7], thus, may have the potential to elevate their SCC susceptibility, leading to CGRs comparable to those typical of Alloy 600. Another remarkable recent study has found that LRO precipitation under proton irradiation was observed for the first time, in alloys C22, 625, 625P, 625D, 725, and 690 [8]. The Fe level in the Alloy 690 heat was 10.38 wt. %, and the irradiation was conducted at 360°C with 2 MeV protons to a damage level of 2.5 dpa.

Overall, the research to date on the effect of aging in Ni-based alloys seems to have been focused almost exclusively on the base alloys, and primarily on model alloys as the investigators sought to gain a fundamental understanding of the mechanisms in play. As a result, research on commercial heats has been extremely scarce and limited to microstructural examinations. As noted previously, with the notable exception of the study by Young et. al [3] on model alloy Ni-33Cr, the effects of those microstructural changes on the SCC response have not been evaluated.

The need for an assessment of the long-term aging effects on the performance in Alloy 690 and associated weldments was identified as a research gap in the Light Water Reactor Sustainability (LWRS) stakeholders report for 2020 [9], and was recognized as a strategic research need by both industry [2, 10] and regulators [11]. Hence, a research program was initiated at Argonne in 2020 to address that need and bridge the gap between the microstructural examination and performance testing.

In order to study the effect of aging on performance, ANL produced an Alloy 152 dissimilar metal weld joining Alloy 690 and Alloy 533 LAS in 2011, identical to the one developed and produced for the US NRC program in 2010, which was then aged up to 75,000h over the following nine years, to 30 and 60-year service equivalents. This creates the opportunity to examine the effects of aging in several pedigreed alloys that have been characterized and tested extensively at ANL and worldwide in the un-aged condition over the past decade.

In its first year, the Argonne program focused on the microstructural evolution and the SCC response of Alloy 690 under accelerated thermal aging and irradiation conditions [12]. In addition to the aged Alloy 690, the study also involved specimens neutron-irradiated in the BOR-60 reactor up to 40 dpa. For aged Alloy 690 specimens, hardness was found to increase with aging time, however, the microstructural characterization by means of synchrotron X-ray did not find evidence of LRO. The microstructural characterization of neutron-irradiated specimens by TEM found no evidence of LRO either. Testing in a primary water environment of Alloy 690 specimens aged to a 60-year service equivalent revealed a fatigue and corrosion fatigue crack growth responses similar to those measured on the un-aged alloy. The SCC CGR response was also low. Overall, the two Alloy 690 heats investigated in this work, aged up to 60-year service equivalents or exposed to neutron irradiation up to 40 dpa, did not exhibit a deterioration in microstructure or performance.

The current research – summarized in this report - was focused on the microstructural evolution and the SCC response of Alloy 152 under accelerated thermal aging.

Chapter 2 describes the weld mockup used in the aging study, including the materials of fabrication, the schematic design of the welds, and the weld fabrication processes. One of the objectives for this weldments was that the materials and welding parameters be representative of those used for actual welds used in service. Chapter 2 also presents the equipment used in the microstructural examinations. The crack growth testing equipment and experimental approach are also presented. ANL generally followed a well-established testing protocol that has been employed for a number of years and was reported in previous ANL reports.

Chapter 3 provides findings of the microstructural examinations and the results of the crack growth rate tests. Complete CGR data sets are provided as a function of testing conditions, and presented as crack advance vs. time plots.

Chapter 4 provides a discussion of the testing results in the framework provided by the well-established fatigue and corrosion fatigue behavior for these alloys, as well as the industry-proposed disposition curves for crack growth [1]. Finally, Chapter 5 gives a summary of the main findings and conclusions.

2 Experimental

This section describes the alloys used in this study, the equipment used for microstructural analysis, the configuration of test specimens for crack growth rate (CGR) testing, and the CGR test apparatus and experimental approach.

2.1 Alloys

The alloys used in this work came from weldment that was aged to 30-year and 60-year service equivalents. Since the microstructural investigation was focused on LRO, a model alloy Ni-33Cr – with known susceptibility to LRO - was also included in the investigation.

2.1.1 Alloy 152 weld produced by ANL (Alloy 690 to Alloy 533 Grade B Joint)

The research presented in this report focuses on aged Alloy 152 which was part of a weldment, hence, for completeness, this section presents the all the component materials and steps undertaken to produce the weldment.

The Alloy 690 (Heat NX3297HK12) was received from Nuclear Alloy Corp. in a plate form that was 6.4-cm (2.25-in.) thick x 7.6-cm (3-in.) wide x 86.4-cm (34-in.) long. The designation for the metallurgical condition of the as-received plate was MIL-DTL-24802. To reach this condition, the alloy was vacuum-induction-melted, electro-slag-remelted, hot-rolled, de-scaled, and annealed at 1038°C (1900°F) for 2 h, then air-cooled. The chemical composition provided by the vendor, as well as that determined at ANL by inductively-coupled plasma optical emission spectrometry (ICP-OES), is reported in Table 1.

Table 1 Chemical composition (wt. %) of Alloy 690 (Heat NX3297HK12) plate.

Alloy ID (Heat)	Analysis	C	Mn	Fe	S	P	Si	Cu	Ni	Cr	Ti	Nb	Co
A 690WC (NX3297HK12)	Vendor	0.03	0.20	9.9	<0.001	-	0.07	0.01	59.5	29.5	-	-	-
	ANL	0.04	0.33	8.53	0.001	0.003	0.02	0.04	59.67	30.82	0.47	0.01	<0.01

The Alloy 690 plate was used to produce a 3-inch thick Alloy 152 butt weld to SA-533 Gr B class 1 steel (Heat A5466-2 from the Midland reactor lower head [13]) buttered with Alloy 152 filler metal. The geometry of the joint is shown in Figure 1. The joint was designed with a straight edge on the Alloy 690 side to facilitate SCC CGR testing of the Alloy 690 heat affected zone (HAZ). The SMAW welding procedure was qualified to ASME Section IX by ANL Central Shops [14].

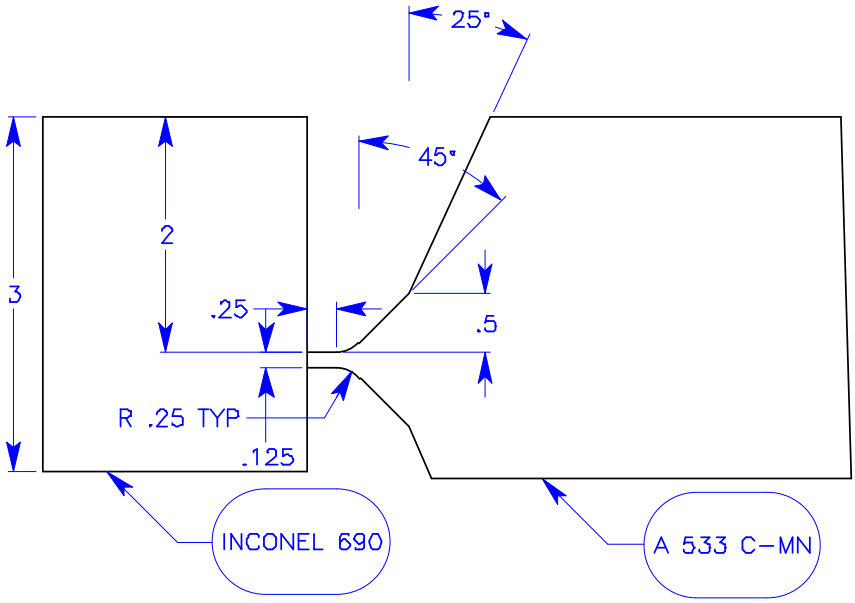

Figure 1 Joint design, Alloy 690 to SA-533 Gr B. Units are in inch.

2.1.1.1 Alloy 152 Weld Buttering

The LAS plate was machined with a bevel on one end. The beveled end was buttered with Alloy 152 F43 filler metal. A record was kept of the number and location of weld passes together with the heat code of the filler metal used, and the welding parameters that were used, Table 2 [14]. This record is shown in [14]. After each layer, a liquid penetrant (LP) check was performed. After buttering, the LAS piece was stress relieved at 1150 ± 25ºF for 3h. The chemical composition of the Alloy 152 filler heat 720129 that was used to produce the first layer of buttering is given in Table 3.

Table 2 Welding process and conditions for various weld passes used for fabricating the Alloy 152 butter

Weld Pass	Process	Filler Metal	Filler Size, in.	Heat Code	Type Polarity	Current, A	Voltage, V	Travel Speed, in./min	Notes
1 – 23	SMAW	Alloy 152, EniCrFe-7	1/8	720129	DCRP	97-102	21 – 23	5	Layer 1 LP
24-44	SMAW	Alloy 152, EniCrFe-7	5/32	146444	DCRP	113-117	25 – 26	5	Layer 2 LP
45-65	SMAW	Alloy 152, EniCrFe-7	5/32	146444	DCRP	113-117	25 – 26	5	Layer 3 LP

DCRP = direct current reverse polarity

Table 3 Chemical composition (wt. %) of Alloy 152 heats used to produce the weld buttering

Alloy ID	Analysis	C	Mn	Fe	S	P	Si	Cu	Ni	Cr	Ti	Nb+Ta	Co
A152 (720129)	CMTR	0.037	3.70	9.28	<0.001	<0.003	0.51	0.01	55.26	28.92	0.12	1.92	<0.01
A152 (146444)	CMTR	0.040	3.56	9.36	<0.001	<0.003	0.46	<0.01	55.25	29.04	0.15	1.84	<0.01

2.1.1.2 Alloy 152 Butt Weld

The buttered LAS piece described in the previous sub-section was beveled on the buttered edge leaving ¼" of Alloy 152 F43 weld material on the face, and a section of Alloy 690 plate was used to make the opposing part of the butt weld. A double bevel J-grove weld was produced according to the design shown in Figure 1, and the number and location of weld passes together with the heat code of the filler metal used, as well as the welding parameters are given in Table 4. The root pass of the weld and back grind was LP tested, and the final weld surface was also LP tested. The final weld was radiographed per ASME Section IX. The resulting weld along with its component heats is shown in Figure 2 and Figure 3. The chemical composition of the Alloy 152 filler heat WC04F6 that was used to complete the butt weld is given in Table 5.

Table 4 Welding process and conditions for various weld passes used for fabricating the A152 butt weld

Weld Pass	Process	Filler Metal	Filler Size, in.	Heat Code	Type Polarity	Current, A	Voltage, V	Travel Speed, in./min	Notes
1 – 8	SMAW	Alloy 152, EniCrFe-7	1/8	720129	DCRP	97-102	21 – 23	5	
9-14	SMAW	Alloy 152, EniCrFe-7	1/8	146444	DCRP	97-102	25 – 26	5	Root LP BG LP
15-26	SMAW	Alloy 152, EniCrFe-7	5/32	146444	DCRP	113-117	25 – 26	5	Final LP
27-76	SMAW	Alloy 152, EniCrFe-7	1/8	WCO4F6	DCRP	97-102	25 – 26	5	Final LP

DCRP = direct current reverse polarity

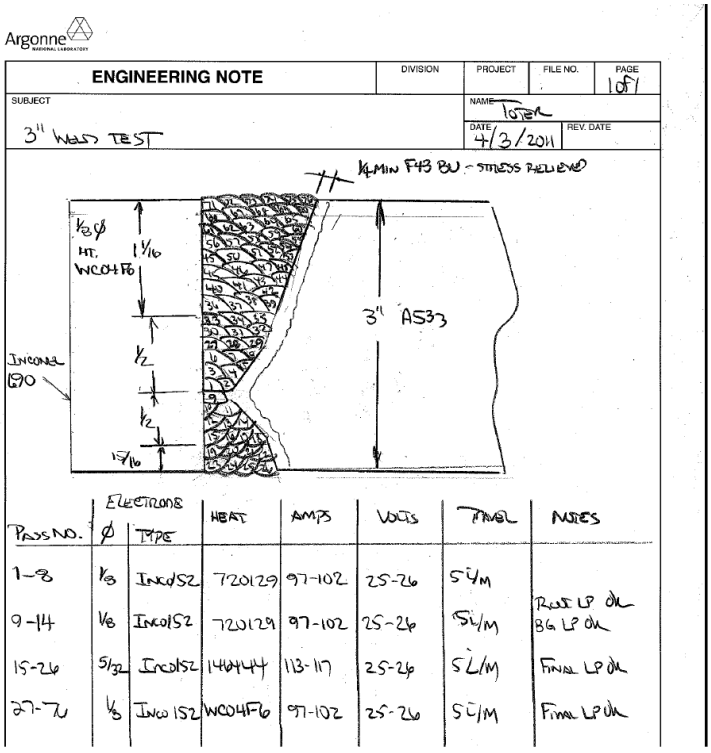

Figure 2 Schematic of the Alloy 152 weld joining Alloy 690 and Alloy 533 produced for aging in 2011. The weld was produced in an identical fashion using the same materials and procedures used to produce the weld for the US NRC program a year earlier. The table below the weld schematic shows the Alloy 152 weld heats and welding parameters.

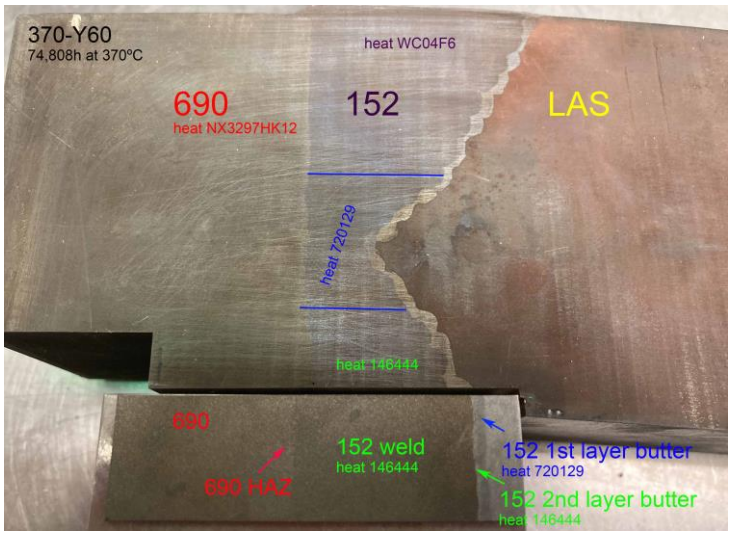

Figure 3 **Alloy 152 weld joining Alloy 690 and Alloy 533 aged to a 60-year service equivalent. The three Alloy 152 weld heats are identified.**

Table 5 **Chemical composition (wt. %) of Alloy 152 heat WC04F6 used to complete the butt weld**

Alloy ID (Heat)	Analysis	C	Mn	Fe	S	P	Si	Cu	Ni	Cr	Ti	Nb	Co
A152 (WC04F6)	CMTR	0.048	3.48	10.39	0.003	0.003	0.41	<0.01	55.20	28.70	0.09	1.54	<0.005
	ANL	-	3.88	9.56	-	<0.08	0.52	<0.04	53.70	28.40	0.10	1.80	<0.04

2.1.2 Prior characterization and testing of the un-aged Alloy 152 to Alloy 533 Grade B Joint

One of the main advantages of using the weldment described in this section for an aging study is the existence of a large database for benchmarking. The non-aged material from the sister weldment have been tested extensively at ANL under an US NRC program [15-17] and elsewhere. Some key findings are as follows:

Alloy 690:

- Alloy 690 Heat NX3297HK12 was the original material used by ANL in 2006 to show that 26% cold work promotes SCC growth in Alloy 690. The material was shared with several other laboratories and was tested extensively worldwide. Notably, 11% - the most from any one heat - of the data points in the MRP-386 database [2] were obtained using this heat. Alloy 690 Heat NX3297HK12 has a Fe content below 10 wt. % (9.9 and 8.53 wt. % in two independent measurements, Table 1), so it could be prone to developing LRO under long term exposure. However, the microstructural characterization conducted in this program by means of synchrotron X-ray did not find evidence of LRO in specimens aged to 60 year of service equivalents [12]. Nevertheless, as described previously, aging to a 80-year service equivalent is in progress.

The Alloy 152 weldment was produced with three heats:

- Alloy 152 Weld Heat WC04F6 was used in the upper J-weld. It was tested extensively at ANL [15, 17] and elsewhere, and significant IG SCC was developed routinely in testing, resulting in moderately-high SCC CGRs, Figure 4. It is the most SCC-susceptible weldment in the MRP-

386 database [2]. Alloy 152 Weld Heat WC04F6 has a Fe content of 10.39 wt. % (Table 5), so it would be less prone to the formation of LRO under long term exposure.

- Alloy 152 Weld Heat 720129 was used to weld on both sides of the root. It has not been tested as part of the weld, but was tested as the first buttering layer on Alloy 533 LAS. Alloy 152 Weld Heat 720129 has a Fe content of 9.28 wt. % (see Table 3), so it would be prone to LRO formation under long term exposure.
- Alloy 152 Weld Heat 146444 was used to complete the bottom J-weld. It has not been tested as part of the weld, but was tested as the second buttering layer on Alloy 533 LAS. Alloy 152 Weld Heat 146444 has a Fe content of 9.36 wt. % (see Table 3), so it would be prone to LRO formation under long term exposure.

The Alloy 152 butter was produced with two heats (Table 3):

- Alloy 152 Weld Heat 720129 was used as a first layer butter on Alloy 533 LAS. It has been tested extensively at ANL [16] and elsewhere. In SCC CGR testing, this weldment produced fully IG-engaged crack fronts, and very high rates, Figure 5 [16]. The weldment and tested specimens were examined extensively at ANL and worldwide. Alloy 152 Weld Heat 720129 has a Fe content of 9.28 wt. % (see Table 3), so it would be prone to LRO formation under long term exposure.
- Alloy 152 Weld Heat 146444 was used as a second layer butter on the Alloy 533 LAS and was tested in that configuration. This weldment was found to be resistant. Alloy 152 Weld Heat 146444 has a Fe content of 9.36 wt. % (see Table 3), so it would be prone to LRO formation under long term exposure.

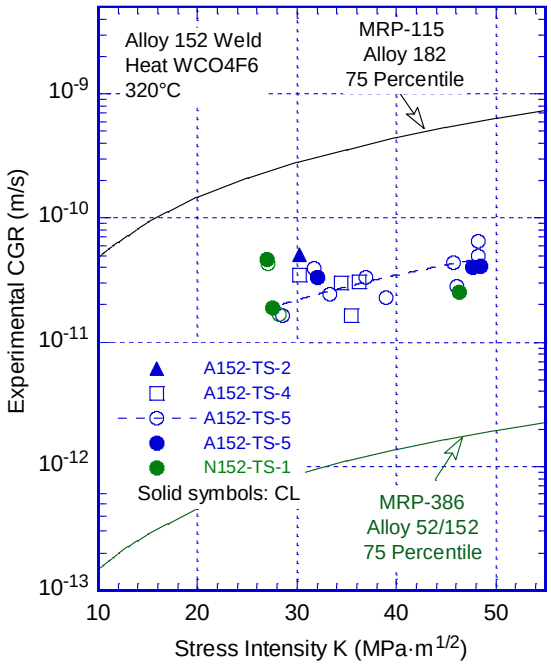

Figure 4 **SCC CGRs for Alloy 152 weld heat WC04F6 [15, 17]. Solid symbols represent SCC CGRs measured under constant load (CL) and open symbols represent SCC CGRs measured under periodic partial unloading (PPU) conditions. The proposed disposition curves for Alloys 182 [1] and 52/152 [2] are included.**

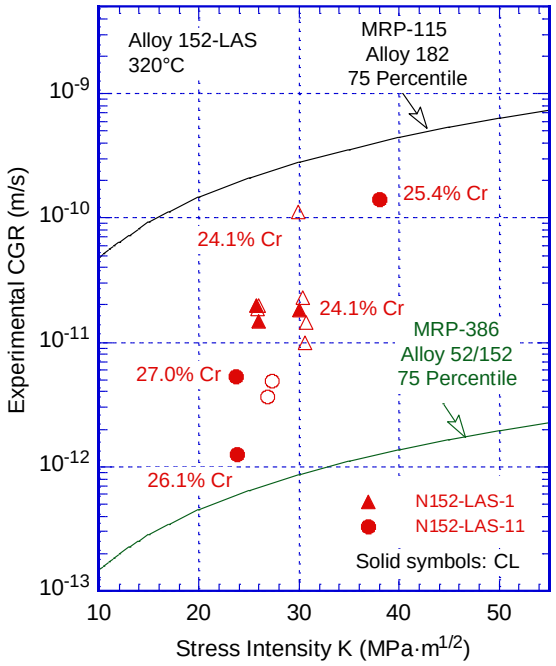

Figure 5 **SCC CGRs for 1st layer of Alloy 152-LAS weld heat 720129 [16]. Cr-concentrations measured along the crack path in the regions where the rates were determined are shown in the figures. Solid symbols represent SCC CGRs measured under constant load (CL) and open symbols represent SCC CGRs measured under periodic partial unloading (PPU) conditions. The proposed disposition curves for Alloys 182 [1] and 52/152 [2] are included.**

This weldment was also made available to collaborators from Korea, and the microstructure of the Alloy 152 weld, particularly the butter, was examined extensively in the non-aged and intermediate aged conditions [18, 19].

2.1.3 Aging of the Alloy 690 to Alloy 533 Grade B Joint

In order to emulate the thermal exposure at temperatures of 320°C during 30-year and 60-year service lifetimes of a component, this study employed an accelerated aging approach. The aging conditions were determined using the following equation:

$$\frac{t_{aging}}{t_{ref}} = \exp\left[-\frac{Q}{R}\left(\frac{1}{T_{ref}} - \frac{1}{T_{aging}}\right)\right] \quad (1)$$

where t_{aging} is the aging time (h), t_{ref} is the service time at operation temperature (h), T_{aging} is aging temperature (K), T_{ref} is operation temperature (K), R is the gas constant, and Q is the activation energy.

The 30-year and 60-year year service equivalents were estimated for three aging temperatures (370°C, 400°C, and 450°C) using Eq. (1) with an activation energy of 125 kJ/mol, in excellent agreement with the Framatome/EdF estimate for LRO formation [6], and the results are shown in Figure 6. The figure also includes a photograph of the actual aged weld pieces. The maximum accelerated aging temperature

was 450°C to prevent the formation of microstructural phases atypical of normal operating conditions, such as excessive carbides or sigma phases. Specimens are designated by "temperature – service equivalent", for example specimen "400-Y60" was aged at a temperature of 400°C to reach a 60-year equivalent exposure at 320°C.

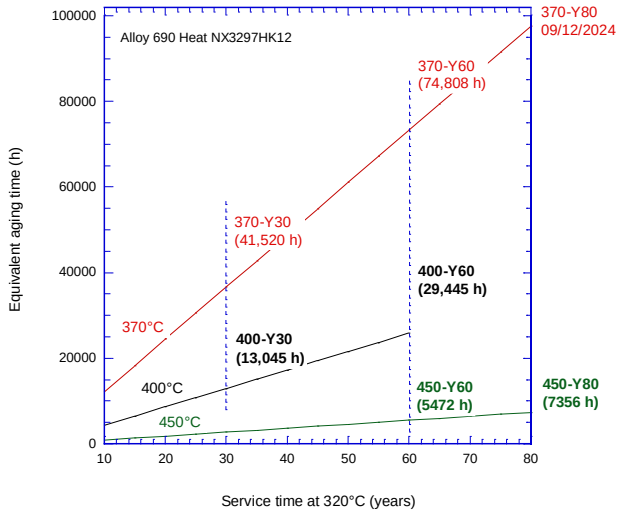

(a)

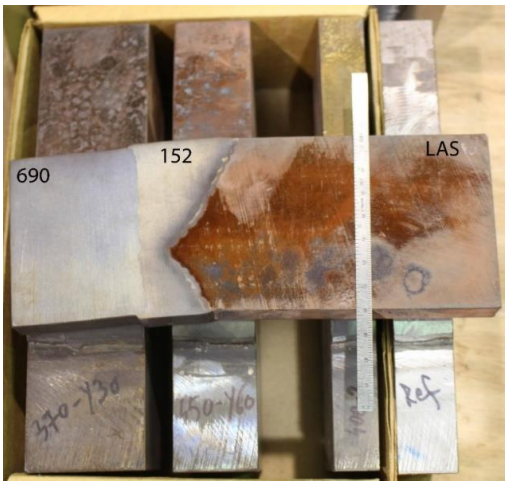

(b)

Figure 6 **(a) Diagram showing the total hours for each aging temperature (370°C, 400°C, and 450°C). Estimates for 30-year and 60-year service equivalents calculated using Eq. (1) with an activation energy of 125 kJ/mol. The diagram also includes the actual aging times. Weld pieces are currently aged to 80-year service equivalent. (b) photograph of the actual pieces of Alloy 152 weld joining Alloy 690 and Alloy 533 that were aged.**

2.1.4 Model Ni-33Cr Alloy

Given that model alloys tend to develop LRO readily (see for example ref. [3]), a piece of model alloy with demonstrated LRO history [21] was obtained for this program from Dr. S.S. Kim of KAERI, Korea. The Ni-33Cr plate was made by vacuum induction melting followed by hot rolling at 1200°C, solution annealing at 1050°C for 1 h and water quenching. At ANL, this solution-annealed alloy was subjected to two different aging treatments at 475°C known to induce LRO [3]. The intent is to use these conditions as reference for the material characterization effort undertaken in this program which involves commercial heats.

2.2 Microstructural Characterization

The microstructural characterization involved hardness testing as well as analytical techniques such as diffraction at ANL APS or in a TEM focusing on detecting LRO.

2.2.1 X-ray Diffraction at Argonne APS

X-ray diffraction experiments were undertaken at ANL APS with the purpose of detecting LRO in aged Alloy 690 specimens. A similar evaluation has been undertaken previously at ANL APS on a model Ni-33Cr alloy where LRO occurs readily, in as little as 240h under thermal exposure of 475°C [21]. For example, Figure 7 (taken from ref. [21]) shows synchrotron X-ray diffraction peaks from Ni-33Cr alloy in water-quenched and aged conditions. The initial portions of the respective spectra are magnified and

are shown as inserts in each figure. In addition to the expected FCC peaks that are present in all alloy conditions, figures (c) and (d) exhibit peaks - indexed with red – typical of Pt_2Mo-type domains. These Pt_2Mo superlattice peaks with d-spacings of 3.76 Å, 3.24 Å, and 2.38 Å were indexed as the (020), (011), and (110) of the body-centered orthorhombic (BCO) structure, and indicate the occurrence of Pt_2Mo-type ordering, i.e., LRO in aged samples.

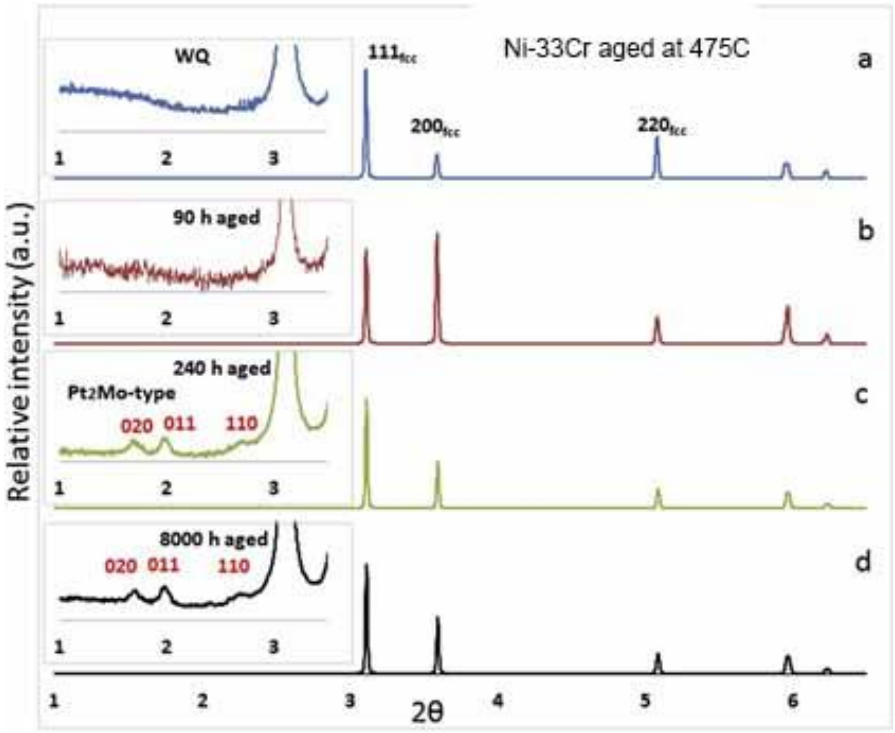

Figure 7 **Synchrotron X-ray peaks from Ni-33Cr alloy (a) water-quenched alloy (b) 90 h aged (c) 240 h aged (d) 8000 h aged. Initial portions of the respective spectra are magnified and are shown as insets. In addition to the FCC peaks that are present in all alloy conditions, (c) and (d) show peaks (indexed with red) from Pt_2Mo-type domains (taken from ref. [21]).**

For the present research, the X-ray diffraction experiment was performed at the 1-ID beamline of the APS, and the experimental details are summarized in Table 6. The detectors were calibrated with a CeO_2 powder sample (NIST standard SRM674b). All the samples were nominally 1-mm thick. For the weld samples, spot measurements were performed at the three Alloy 152 weld heats (refer to Figure 3). Figure 8 is a photo showing the actual beamline setup; note the three red marker dots on the sample plate indicating the measurement points on the three heats. At each measurement point, during the exposure, the sample rocked ±1.5°. This approach maximized the diffraction signal coverage in the azimuthal direction that the detector collected to create powder-like diffraction patterns for high-fidelity data analysis. A line scan was also performed for each weld sample, traveling from the Alloy 690 to the LAS with the thinnest weld section; in Figure 8 this corresponds to the right edge of the lead tape that was stuck to the sample. For the Ni-33Cr model alloy samples, spot measurements were performed with the same ±1.5° rocking method. The 2D diffraction patterns were transformed into intensity maps of azimuth angles versus radial positions, and were integrated in the azimuthal direction to create the 1-D diffraction profiles for phase identification.

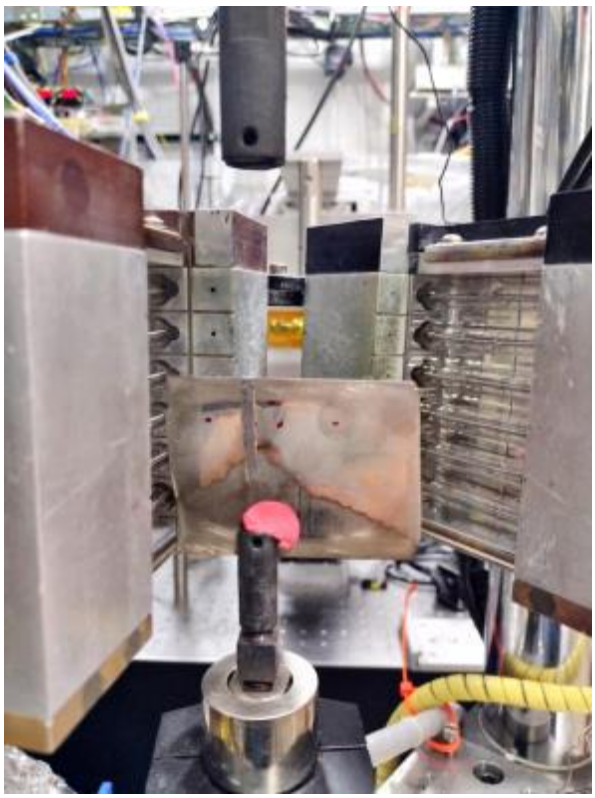

Figure 8 Experimental setup at the beamline for analyzing the weld material.

Table 6 Experimental details for the X-ray diffraction conductucted at ANL APS on aged Alloy 152 and Ni-33Cr specimens.

Material	Condition	X-ray Energy (keV)	Beam size (mm^2)	Distance sample-detector (mm)
A690 to LAS weld	reference	71.676	0.1 x 0.1	870
A690 to LAS weld	370°C-Y60	71.676	0.1 x 0.1	870
A690 to LAS weld	450°C-Y60	71.676	0.1 x 0.1	870
Ni-33Cr model alloy	reference	71.676	0.1 x 0.1	870
Ni-33Cr model alloy	475°C, 200h	71.676	0.1 x 0.1	870
Ni-33Cr model alloy	475°C, 2000h	71.676	0.1 x 0.1	870

2.3 SCC Crack Growth Rate Testing

2.3.1 Compact tension (CT) Specimens

The tests conducted under this project were performed on ½-T compact tension (CT) specimens; the geometry of the CT specimens is shown in Figure 9. The CGR tests were conducted in simulated PWR environments at 320°C. The testing protocol was in accordance with ASTM E-647, "Standard Test Method for Measurement of Fatigue Crack Growth Rates," [22] and ASTM E-1681, "Standard Test Method for Determining a Threshold Stress Intensity Factor for Environment-Assisted Cracking of Metallic Materials under Constant Load" [23].

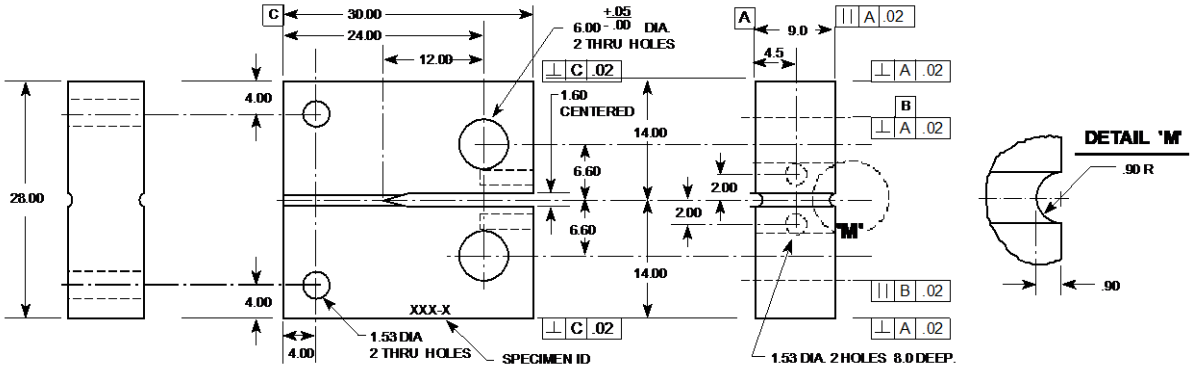

Figure 9 Configuration of the ½-T CT specimen used for this study. Dimensions are in mm.

PWSCC Crack Growth Test Facilities

The CGR tests were conducted in test facilities equipped with either 2 or 6-liter stainless steel (SS) autoclaves. Each system has a suite of calibrated instrumentation, including digitally controlled hydraulic loading and load cells, and an independent water loop to maintain a simulated PWR environment with water chemistry monitoring. The test systems are nearly identical except for the maximum load rating of the test frame and the volume of the autoclave vessel. A detailed description of the test system with the 2-liter autoclave is provided in this section.

The 2-liter autoclave test facility allows test temperatures of up to 350°C. Figure 10 is a photograph showing the entire test system. The servo-hydraulic test frame consists of a load train, an autoclave support frame, and autoclave. The hydraulic actuator is mounted on bottom of the test frame, with the load train components located above it. The load cell is located at the bottom of the pull rod. An Instron Model 8800 system is used to control the load on the specimen. The test temperature is maintained by heater bands mounted on the autoclave body.

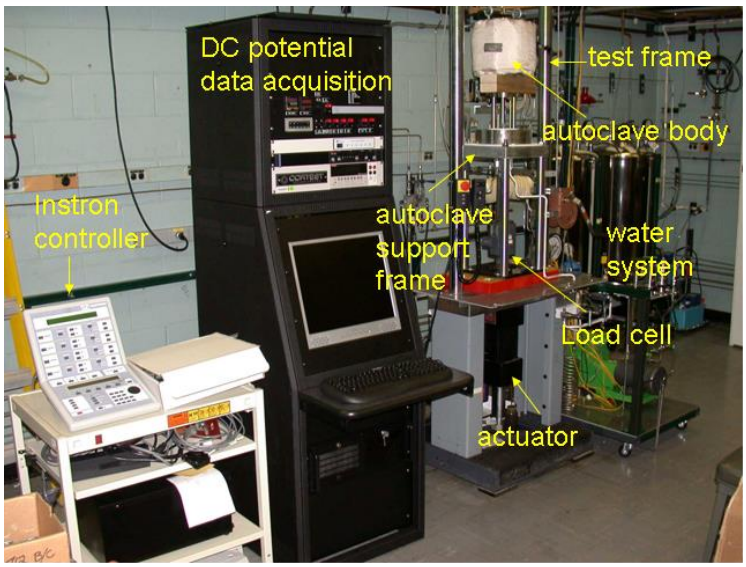

Figure 10 Layout of the 2-liter SCC test system.

The autoclave support frame consists of a thick plate supported by four compression rods (Figure 11). The internal load frame that contains the test specimen consists of a top plate supported by three rods. The upper two-piece clevis assembly is fastened to the top plate of the internal load frame, and the lower piece clevis assembly is connected to the pull rod. The specimen to be tested is mounted between the clevises. The specimen and clevises are kept electrically insulated from the load train by using oxidized Zircaloy pins and mica washers to connect the clevises to the rest of the load train. Water is circulated through a port in the autoclave head, which serves both as inlet and outlet. A schematic diagram of the recirculating water system is shown in Figure 12.

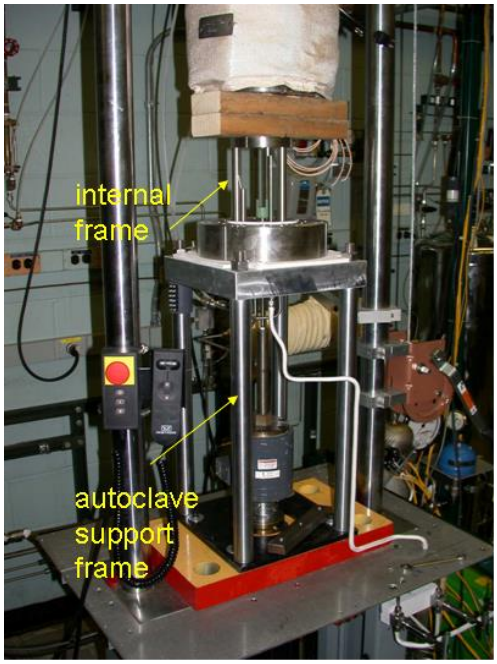

Figure 11 Photograph of the specimen load train for the 2-liter autoclave.

The simulated PWR feedwater contains 2 ppm Li as LiOH, 1000 ppm B as HBO_3, ≈2 ppm dissolved hydrogen (≈23 cm^3/kg), and less than 10 ppb dissolved oxygen (DO) [24]. Water is circulated at relatively low flow rates (15-25 mL/min). The test temperature was 320°C.

Crack extensions are monitored by the reversing-direct current (DC) potential difference method, Figure 13. In this method, a constant DC current is passed through the test specimen and the crack length is measured through the changes in the electrical voltage at the crack mouth. The electrical voltage measured across the crack mouth is related to the unbroken crack ligament resistance through the Ohm's law. Thus, as the crack advances, the length of the unbroken ligament decreases and its resistance increases. In short, as the crack advances the voltage measured across the crack mouth increases. Figure 13 shows a typical configuration of a CT specimen instrumented for crack growth measurements by the DC potential method: the current leads are welded on the top and bottom surfaces of the specimen, and potential leads are welded on the front face of the specimen across the machined notch but on diagonal ends. Also, to compensate for the effects of changes in resistivity of the material with time, an internal reference bar of the same material being tested is installed in series, near the test specimen. The voltage readings across the reference bar are used to normalize potential drop measurements for the CT test specimen. The changes in potential drop measurements for the CT test specimen are transformed into crack advance data using correlations developed for the specimen geometry that is tested. In practice, voltage readings are taken successively as the current is reversed, and, typically, 800 voltage readings are needed to generate 1 crack advance data point, approximately every 4 min. with a resolution of approximately 1-2 μm [0.039-0.079 mils].

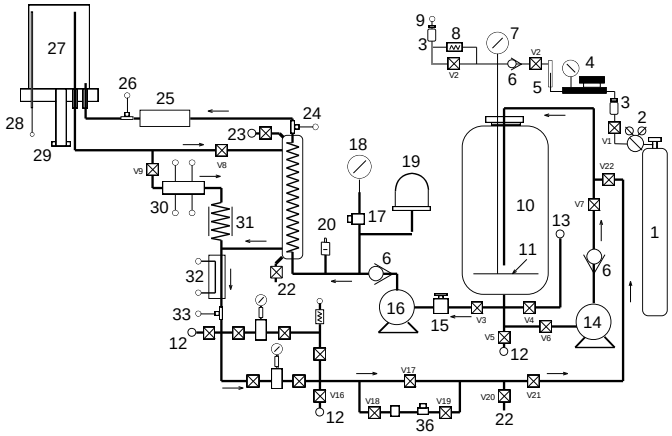

1. COVER GASS SUPPLY TANK
2. TWO-STAGE HIGH-PRESSURE REGULATOR
3. FLASH ARRESTOR
4. LOW-PRESSURE REGULATOR
5. FLOW METER
6. CHECK VALVE
7. COMPOUND VACUUM & PRESSURE GAUGE
8. PRESSURE RELIEF VALVE
9. VENT TO AIR & FLASH ARRESTOR
10. FEEDWATER STORAGE TANK
11. SPARGE TUBE
12. WATER SAMPLE PORT
13. FEEDWATER FILL PORT
14. FEEDWATER TANK RECIRCULATION PUMP
15. SOLENOID VALVE
16. HIGH-PRESSURE PUMP
17. PRESSURE TRANSDUCER
18. HIGH-PRESSURE GAUGE
19. ACCUMULATOR
20. RUPTURE DISC
21. HEAT EXCHANGER (HX)
22. DRAIN
23. SYSTEM BLEED PORT
24. HEAT EXCHANGER OUTLET TC
25. AUTOCLAVE PREHEATER
26. PREHEATER OUTLET TC
27. COMMERCIAL AUTOCLAVE
28. THERMOWELL
29. "BAL SEAL" RETAINER
30. ECP CELL
31. AIR-COOLED COIL
32. WATER COOLED HEAT EXCHANGER
33. BACK-PRESSURE REGULATOR (BPR) INLET TC
34. BPR
35. PH METER
36. CONDUCTIVITY METER

Figure 12 Schematic diagram of the recirculating 2-liter autoclave system.

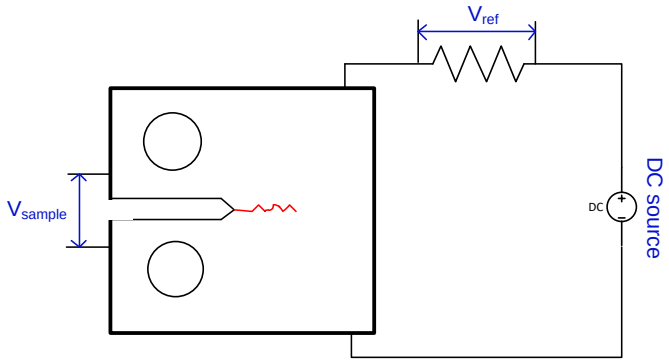

Figure 13 Principle of crack length measurement by the DC potential method.

3 Results

This section describes the findings of the microstructure examination by X-ray diffraction, and the results of SCC CGR testing in a primary water environment. The last subsection contains descriptions for two tests on reference (non-aged) and aged specimens, the latter aged to 60-year service equivalents. The test on reference specimen was conducted under a different research program funded by US NRC and is included here for completeness. The test on the aged specimen was conducted under this program.

3.1 Microstructure

3.1.1 X-ray Diffraction at Argonne APS

Figure 14 presents X-ray Diffraction (XRD) spectra in the three weld heats aged at 370°C and 450°C equivalent to 60 years of service (condition 370-Y60 and 450-Y60). Aged model Ni-33Cr alloy with known LRO [12] was included for reference. For the model alloy, in addition to the FCC peaks that are present in all conditions, the aged conditions show peaks - highlighted with green - from Pt_2Mo-type domains. These superlattice peaks with d-spacings of 3.76 Å and 3.24 Å were indexed as the (020) and (011) of the BCO structure, indicating Pt_2Mo-type ordering in these two samples. By contrast, Alloy 152 heats WC04F6, 720129, and 146444 do not show ordering.

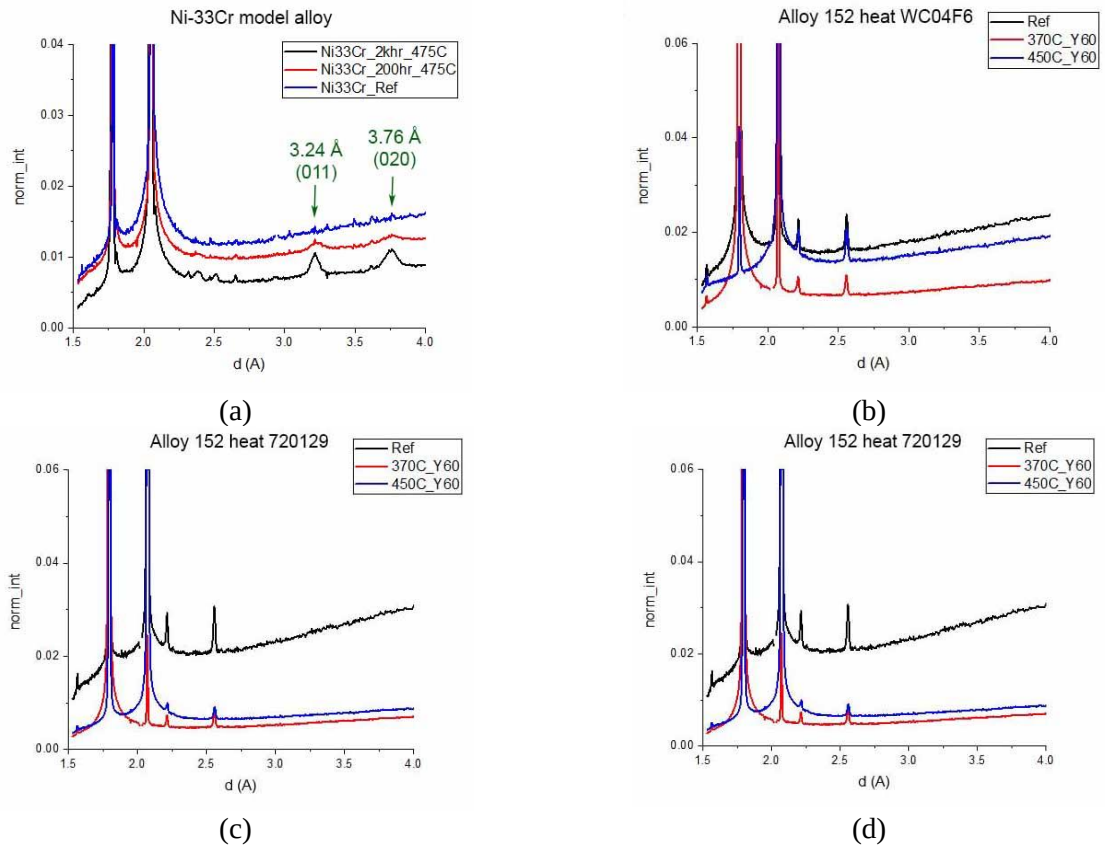

Figure 14 Synchrotron X-ray peaks from (a) Ni-33Cr alloy, (b) Alloy 152 heat WC04F6, (c) Alloy 152 heat 720129, and (d) Alloy 152 heat 146444. Only the aged conditions of model alloy Ni-33Cr show peaks (indexed with green) consistent with Pt_2Mo-type domains.

In addition to the welds, because of their high SCC CGRs (Figure 5), the weld butters are also of high interest. Figure 15 shows an initial evaluation for LRO conducted by Synchrotron XRD in the Alloy 152 butter region of an analysis coupon from the materials condition 370-Y60, aged at 370°C for almost 75,000h, equivalent to 60 years of service. The XRD coupon is shown at the bottom of Figure 3 and is also included for convenience in Figure 15a. The XRD was conducted along the white arrow and spanned a range of alloys in succession: Alloy 533 LAS, Alloy 152 heat 720129 1st layer butter, Alloy 152 heat 146444 2nd layer butter, and Alloy 152 heat 146444 weld. The absence of superlattice peaks with d-spacings of 3.24 Å indexed as the (011) of the BCO structure (see Figure 14a for comparison), suggests that the Pt_2Mo-type ordering has not occurred.

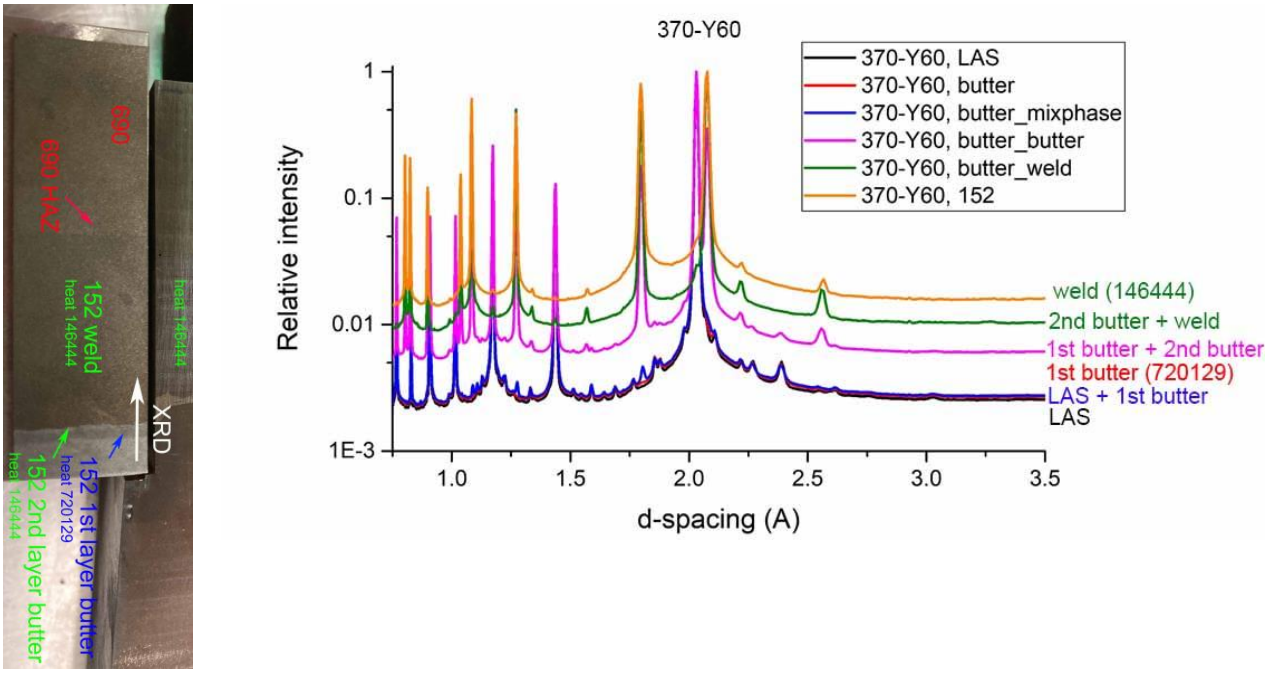

(a) (b)

Figure 15 **(a) XRD analysis coupon spanning the region LAS-Alloy 152 butter-Alloy 152 weld; XRD was conducted along the white arrow. (b) Synchrotron X-ray peaks the regions along the white arrow.**

3.2 PWSCC Crack Growth Rate Testing

3.2.1 Location of SCC CGR test specimens in aged materials and considerations regarding the choice of non-aged specimens for comparison

The first round of SCC testing of aged specimens will involve specimens and heats that have already been tested in the as-welded condition, and have already shown increased susceptibility to SCC, Figure 4 and Figure 5. Given the relative scarcity of aged material, unlike previous testing which involved almost exclusively 1T CTs, the current testing will be conducted on the smaller 1/2T CT to accommodate more specimens and regions of interest. As such, as shown in Figure 16, from one "slice" of aged weld (370-Y60, aged at 370°C for 74,808 h – equivalent to 60 years of service), an Alloy 152 heat WC04F6 (top left) specimen, two Alloy 152 heats 720129 and 146444 in succession (bottom) specimen, and an Alloy 152 heat 720129 in a 1st layer configuration specimen can be tested. The specimen selected to be tested for the program is the Alloy 152 heat WC04F6 (top left), and will be designated 370-Y60 N152. In order to evaluate the effect of aging on the SCC CGR response, a "reference" test will have to be determined.

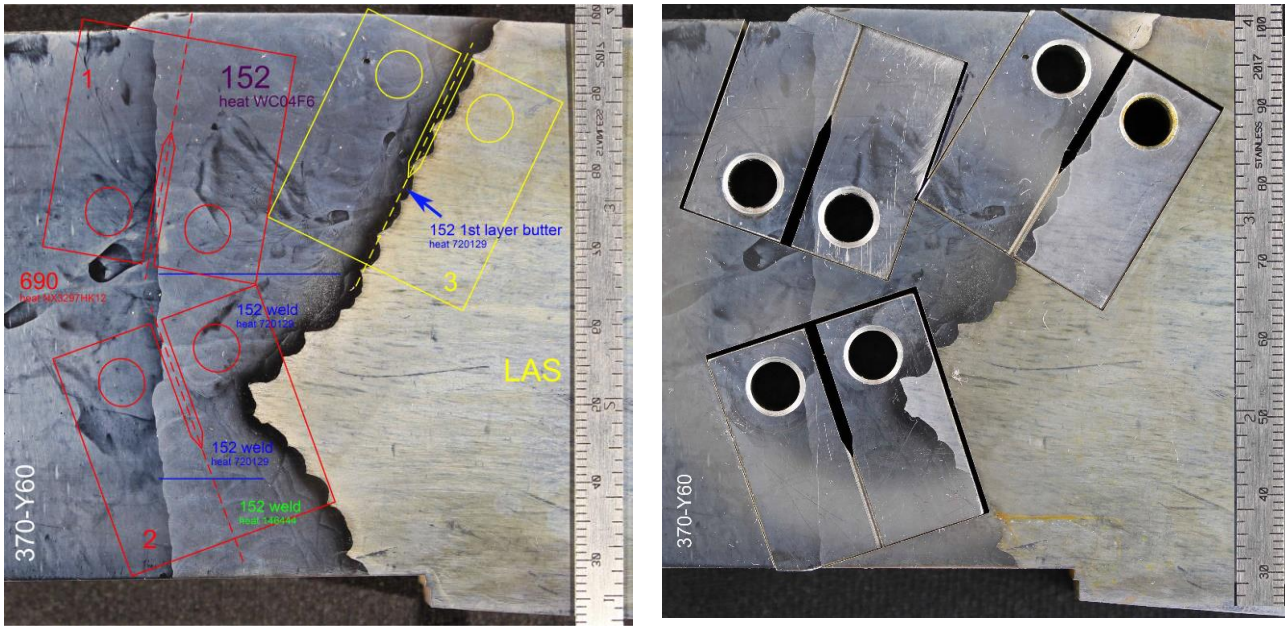

(a) (b)

Figure 16 a) Compact tension (CT) specimens designed to test the Alloy 152 heat WC04F6 (top left), Alloy 152 heats 720129 and 146444 in succession (bottom), and Alloy 152 heat 720129 in a 1st layer configuration. (b) CT specimens ready to be tested.

As described previously, the SCC CGR data for Alloy 152 heat WC04F6 summarized in Figure 4 was obtained using 1T CT specimens positioned in the middle of the weld, Figure 17. In order to maximize symmetry (and growth rate along the dendritic grains) the first weld – designated "A152" - was produced in a double-J geometry, Figure 17a. In the subsequent DMW – designated "N152" – the weldment was produced in a J-groove geometry, yet the specimen was still positioned in the middle of the weld, Figure 17b. Nevertheless, in all cases, SCC CGR testing was initiated in the center, close to

the crown of the weld. In order to accommodate the specimen dimensions, metal pieces had to be eb-welded on top of the existing weld. Specimen N152-TS-1 (Figure 17c) is illustrative of these specimens.

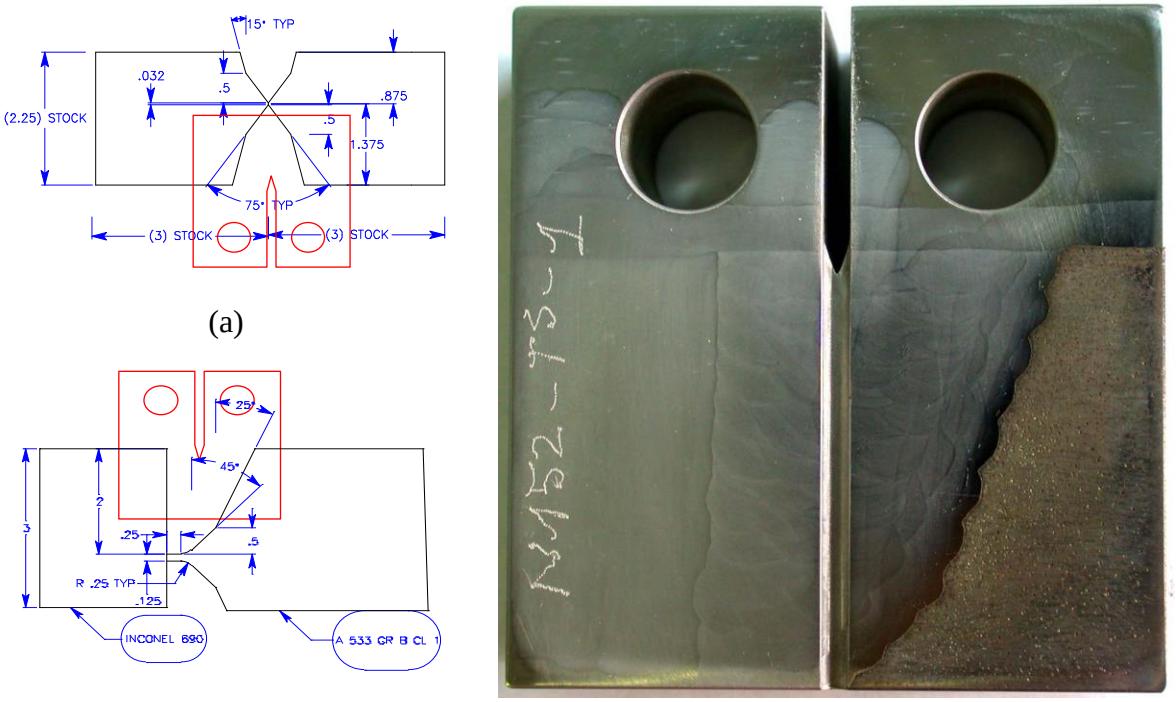

Figure 17 **The orientation of test specimens for Alloy 152 unaged weldments heat WC04F6: (a) double-J weld designated "A152", and (b) J-groove weld designated "N152"; (c) photograph of test specimen N152-TS-1.**

In addition to the tests summarized in Figure 4, Alloy 152 heat WC04F6 was also tested inadvertently in a test intended to evaluate the Alloy 690 HAZ, but the crack ended up in the weld. In that test, the specimen designated CN690-TS-1 was aligned in the HAZ, and was tilted slightly vs. the fusion line to allow the crack to find the weakest path, Figure 18. As it will be described later in this section, the crack entered the weld and sampled this material in a region and orientation very close to that of aged specimen 370-Y60 N152 (see Figure 16).

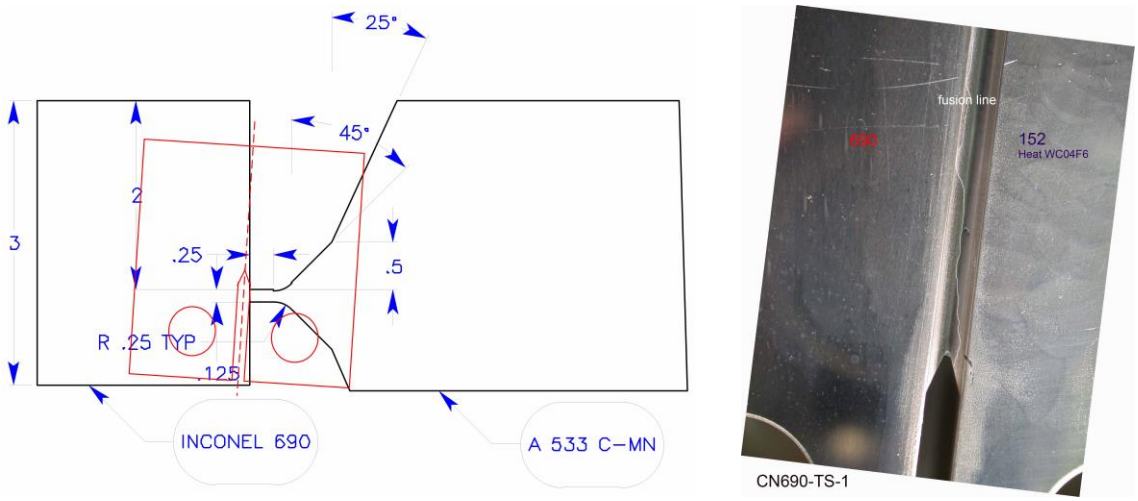

(a) (b)

Figure 18 Specimen CN690-TS-1 aligned to test the Alloy 690 HAZ: a) schematic, and (b) actual specimen.

3.2.2 Crack growth rate testing of Alloy 152 Specimen 370-Y60 N152, aged at 370°C for 74,808 h

The testing conditions for this specimen are given in Table 7, and the changes in crack length and K_{max} with time are shown in Figure 19. Correlations describing cyclic CGRs in air (CGR_{air}) have been established by ANL for Alloy 600, 690, Ni-base weldments as well as SSs [26-30]. The test was initiated in simulated primary water at 320°C with in-situ precracking (Pre a – Pre c), and was followed by transitioning (test periods 1-5). The SCC CGR component evaluated by superposition in test periods 4 and 5 was 1-6 x 10^{-11} m/s, however the response under constant load in period 6 was low; the large decrease in response between test periods 5 and 7 suggests that the crack went off-plane. Environmentally-enhanced conditions were re-established in test period 9 (SCC CGR component evaluated by superposition was 1 x 10^{-11} m/s), then re-evaluated under constant load in test period 10. After two additional SCC CGR determinations in test periods 17 and 18, the crack was advanced in fatigue to a different microstructure, also resulting in a higher stress intensity factor. The transitioning sequence was repeated, and the SCC CGRs were again evaluated in tests periods 22-24 by superposition and directly under constant load. Overall, the SCC CGR response appears similar to that measured in the unaged specimens (Figure 4), in the middle of the weldment.

Table 7 Crack growth data in PWR water[a] for Alloy 152 Specimen 370-Y60 N152 aged for 74,808 h at 370°C

Test Period	Test Time, h	Temp., °C	Load Ratio R	Rise Time, s	Down Time, s	Hold Time, s	K_{max}, MPa·m$^{1/2}$	ΔK, MPa·m$^{1/2}$	CGR_{env}, m/s	Estimated CGR_{air}, m/s	Crack Length, mm
Pre a	4	319.9	0.30	0.5	0.5	0	25.7	18.0	1.23E-07	1.45E-07	11.880
Pre b	5	319.9	0.30	2	2	0	26.0	18.2	3.16E-08	3.75E-08	11.950
Pre c	7	319.9	0.30	5	5	0	26.0	18.2	1.35E-08	1.52E-08	11.989
1	23	319.8	0.50	120	12	0	26.3	13.1	5.35E-10	2.84E-10	12.024
2	50	320.3	0.50	600	12	0	26.4	13.2	1.56E-10	5.83E-11	12.042
3	97	319.8	0.50	1000	12	0	26.4	13.2	8.20E-11	3.49E-11	12.055
4	167	319.2	0.50	1000	12	7,200	26.6	13.3	1.72E-11	4.33E-12	12.061
5	263	319.6	0.50	1000	12	14,400	26.6	13.3	1.47E-11	2.33E-12	12.066

Table 7 (cont.)

Test Period	Test Time, h	Temp., °C	Load Ratio R	Rise Time, s	Down Time, s	Hold Time, s	K_{max}, MPa·m$^{1/2}$	ΔK, MPa·m$^{1/2}$	CGR_{env}, m/s	Estimated CGR_{air}, m/s	Crack Length, mm
6	747	319.8	1.00	0	0	0	26.4	0.0	1.47E-13	-	12.066
7	862	320.9	0.50	1000	12	14,400	26.5	13.2	6.22E-12	2.30E-12	12.068
8	1,030	320.2	0.50	600	12	7,200	26.5	13.3	1.32E-11	4.54E-12	12.075
9	1,103	320.0	0.50	600	12	0	26.4	13.2	1.56E-10	5.80E-11	12.113
10	1,271	320.4	0.50	600	12	7,200	26.5	13.3	1.72E-11	4.56E-12	12.123
11	1,337	320.3	1.00	0	0	0	26.5	0.0	1.41E-12	-	12.126
12	1,353	319.2	0.50	600	12	0	26.3	13.2	1.37E-10	5.66E-11	12.129
13	1,361	319.4	0.50	50	12	0	26.3	13.1	5.32E-10	6.75E-10	12.158
14	1,377	319.3	0.50	600	12	0	26.5	13.2	2.18E-10	5.79E-11	12.169
15	1,384	319.5	0.50	50	12	0	26.6	13.3	1.22E-09	7.13E-10	12.195
16	1,403	319.7	0.50	600	12	0	26.7	13.3	1.63E-10	6.01E-11	12.206
17	1,475	319.3	0.50	600	12	7,200	26.6	13.3	1.60E-11	4.58E-12	12.211
18	1,806	320.1	1.00	0	0	0	26.8	0.0	3.36E-12	-	12.215
19	1,811	320.1	0.30	1	1	0	33.9	23.7	2.01E-07	2.23E-07	13.259
20	1,814	320.1	0.50	50	12	0	34.1	17.1	3.14E-09	1.99E-09	13.316
21	1,831	320.1	0.50	600	12	0	34.3	17.2	4.38E-10	1.70E-10	13.340
22	1,858	320.2	0.50	600	12	7,200	34.3	17.2	5.88E-11	1.31E-11	13.347
23	3,245	319.8	1.00	0	0	0	34.4	0.0	1.30E-11	-	13.358
24	3,459	319.4	0.50	600	12	7,200	34.3	17.2	2.87E-11	1.30E-11	13.386

[a]Simulated PWR water with 2 ppm Li, 1000 ppm B, and 2 ppm H. DO<10 ppb. Conductivity is 21±3 µS/cm, and pH is 6.4.

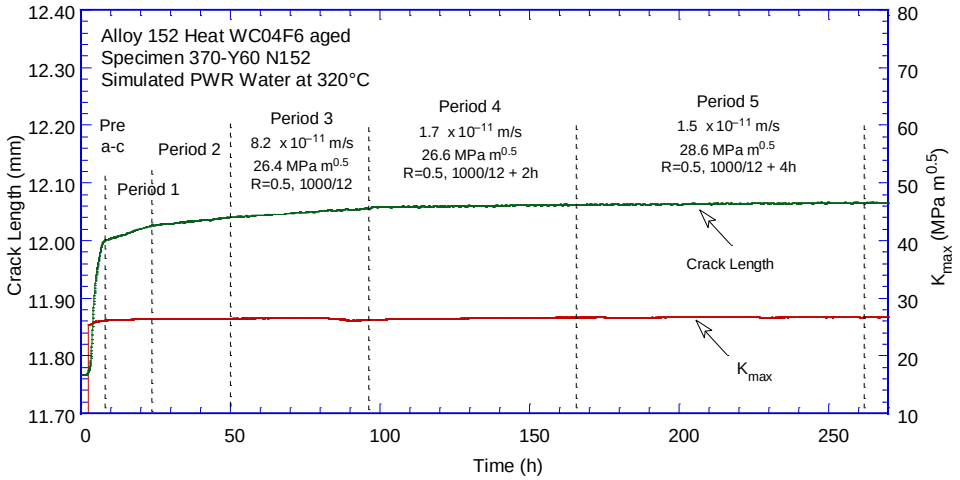

(a)

Figure 19 Crack length vs. time in simulated PWR environment for Alloy 152 Specimen 370-Y60 N152 aged for 74,808 h at 370°C, during test periods: (a) precracking-5, (b) 6-8, (c) 9-15, (d) 16-18, (e) 19-23, and (f) 23-24.

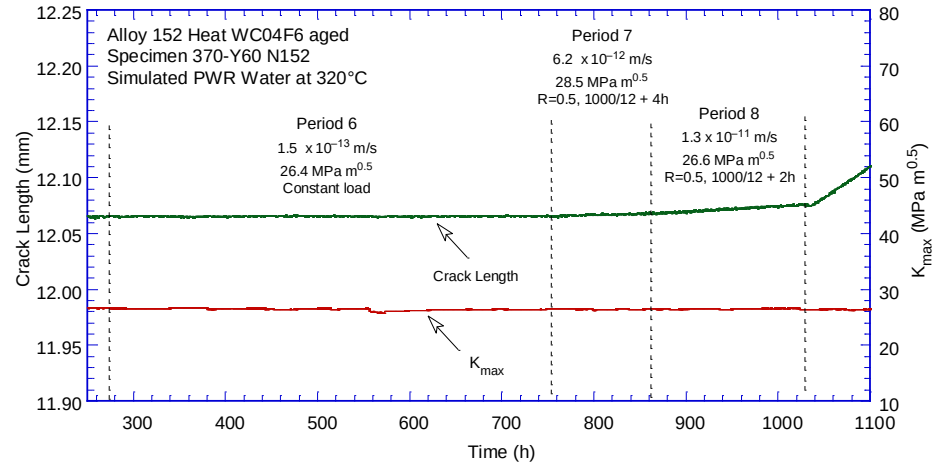

(b)

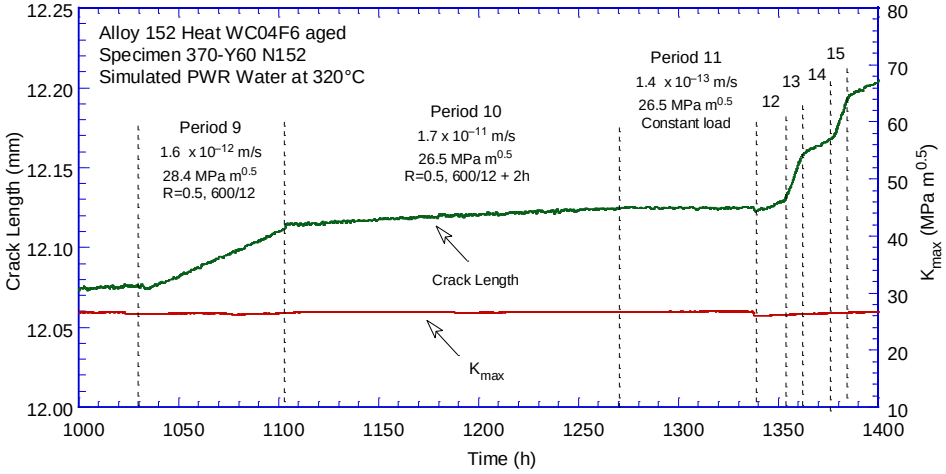

(c)

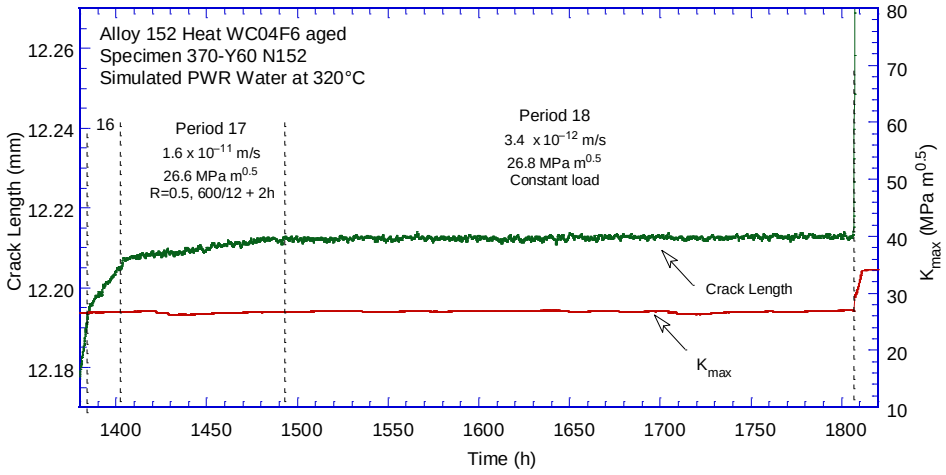

(d)

Figure 19 (cont.)

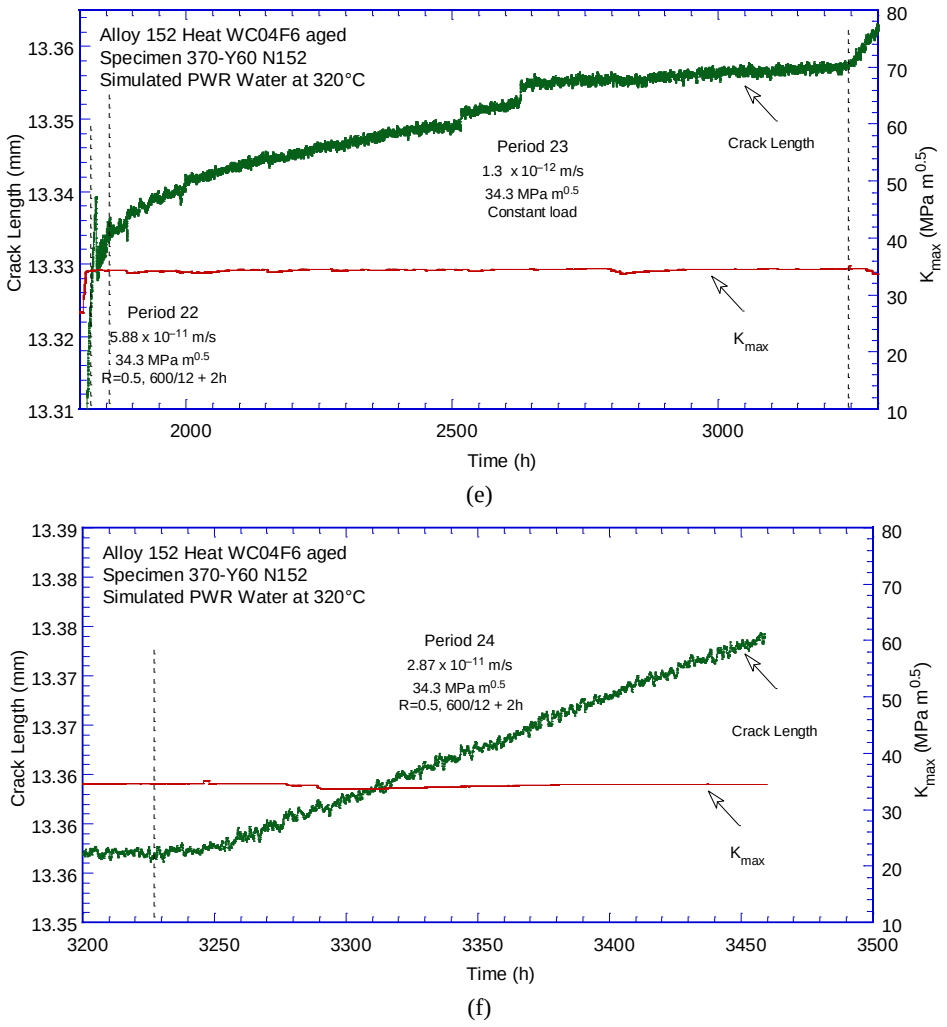

Figure 19 (cont.)

3.2.3 Crack growth rate testing of non-aged Alloy 152 specimen CN690-TS-1

The purpose of this test was to evaluate the SCC CGR response of Alloy 690 HAZ, however, as described previously, Alloy 152 heat WC04F6 was tested instead as the crack ended up in the weld. As it will be described later in this section, the crack entered the weld and sampled this material in a region and orientation very close to that of aged specimen 370-Y60 N152 (see Figure 16), hence could help isolate the effect of aging.

Specimen designated CN690-TS-1 was aligned in the HAZ, and was tilted slightly vs. the fusion line to allow the crack to find the weakest path, Figure 20.

Figure 20 Specimen CN690-TS-1 aligned to test the Alloy 690 HAZ.

The testing conditions for specimen CN690-TS-1 are given in Table 8, and the changes in crack length and K_{max} with time are shown in Figure 21. The CGR_{air} column in the table was modified to reflect the transition to the weld material (red font for the weld rates). The specimen was precracked in the environment, and transitioned in test periods 1-11. The total measured CGR of 4.6 x 10^{-12} m/s in test period 11 is largely identical to the rate expected in air under these loading conditions (4.59 x 10^{-12} m/s), hence essentially no SCC CGR component is present. The rate calculated by superposition in test period 11 was approx. 3.0 x 10^{-12} m/s. The SCC CGR was next measured directly at constant load in test period 19.

Next, more aggressive cycling was used to advance the crack with the expectation that an environmental enhancement would indicate a region with increased susceptibility. The specimen was set at constant load with periodic unloading in test period 27, and then at constant load (test period 28). The measured rate in test period 28 was approx. 1.2 x 10^{-12} m/s.

The crack was further advanced in test periods 29-36. These steps were followed by a test period with a 2h hold, and then constant load in test period 38. After approximately 800 h in this condition the average SCC CGR was 3.6 x 10^{-12} m/s. One final attempt at transitioning was made in test periods 39-

41, and these were followed by a final test period at constant load. As the response diminished to approximately zero growth in the last several hundreds of hours to the test period, the test was ended. Overall, the SCC CGR response appears lower than that measured in the middle of the weld (Figure 4).

Table 8 Crack growth data in PWR water[a] for non-aged Alloy 152 Specimen CN690-TS-1.

Test Period	Test Time, h	Temp., °C	Load Ratio R	Rise Time, s	Down Time, s	Hold Time, s	K_{max}, MPa·m$^{1/2}$	ΔK, MPa·m$^{1/2}$	CGR_{env}, m/s	Estimated CGR_{air}, m/s	Crack Length, mm
Pre a	102	319.9	0.31	1	1		19.0	13.1	7.31E-09	8.53E-09	12.432
Pre b	168	320.1	0.31	100	100		19.1	13.2	3.75E-10	8.57E-11	12.445
Pre c	175	320.4	0.30	1	1		19.2	13.4	1.09E-08	9.15E-09	12.602
Pre d	189	320.1	0.30	50	50		19.2	13.4	8.25E-10	1.83E-10	12.619
Pre e	195	320.9	0.30	1	1		19.4	13.6	1.36E-08	9.51E-09	12.745
Pre f	211	320.8	0.30	50	50		19.4	13.6	8.78E-10	1.92E-10	12.774
Pre g	218	320.9	0.30	1	1		19.6	13.7	1.47E-08	1.01E-08	12.971
Pre h	283	321.0	0.30	50	50		19.7	13.8	7.65E-10	2.06E-10	13.063
Pre i	291	320.7	0.10	1	1		19.9	18.0	2.54E-08	1.95E-08	13.271
Pre j	306	320.3	0.10	50	50		20.1	18.1	1.98E-09	4.00E-10	13.379
Pre k	317	320.6	0.10	1	1		20.6	18.6	2.82E-08	2.23E-08	13.904
Pre l	330	320.1	0.10	50	50		20.9	18.8	3.69E-09	4.67E-10	14.068
Pre m	339	320.4	0.10	1	1		21.5	19.4	3.96E-08	2.67E-08	14.714
Pre n	354	320.0	0.10	50	50		21.7	19.6	4.62E-09	5.52E-10	14.845
Pre o	365	320.0	0.10	1	1		22.7	20.4	4.53E-08	3.27E-08	15.721
Pre p	379	320.2	0.10	50	50		22.9	20.6	3.94E-09	6.86E-10	15.909
Pre q	387	320.5	0.10	1	1		23.5	21.1	3.93E-08	3.81E-08	16.433
Pre r	452	320.2	0.30	50	50		24.0	16.8	1.25E-09	1.09E-09	16.859
1	498	320.4	0.50	50	12		25.2	12.6	6.57E-10	5.72E-10	16.966
2	554	320.5	0.50	300	12		25.2	12.6	1.70E-10	9.61E-11	16.994
3	618	320.1	0.50	600	12		25.2	12.6	9.01E-11	4.80E-11	17.013
4	2,744	319.4	0.50	600	12	7,200	25.4	12.7	8.92E-12	3.75E-12	17.065
5	3,571	319.3	0.5	600	12		26.3	13.2	7.29E-11	5.69E-11	17.273
6	3,763	320.3	0.5	300	12		26.6	13.3	1.61E-10	1.20E-10	17.375
7	4,195	319.7	0.5	600	12	7,200	26.6	13.3	1.03E-11	4.57E-12	17.390
8	4,534	319.8	0.5	300	12		26.4	13.5	1.51E-10	1.16E-10	17.560
9	4,782	320.5	0.5	120	12		26.4	13.4	3.34E-10	2.89E-10	17.838
10	5,118	319.9	0.49	600	12		26.5	13.5	8.43E-11	5.83E-11	17.939
11	5,479	320.3	0.49	600	12	7,200	26.6	13.5	4.63E-12	4.59E-12	17.948
12	6,295	319.0	1	0	0		26.6	13.5	1.52E-12	-	17.958
13	6,535	318.0	0.5	50	12		26.9	13.4	6.55E-10	7.29E-10	18.409
14	6,606	317.8	0.5	600	12		27.0	13.5	1.00E-10	6.16E-11	18.435
15	7,044	319.6	0.5	50	12		28.4	14.2	8.53E-10	9.28E-10	19.471
16	7,110	320.6	0.5	600	12		28.6	14.3	1.26E-10	8.13E-11	19.512
17	7,376	320.2	0.5	50	12		29.7	14.8	1.08E-09	1.12E-09	20.346
18	7,473	320.9	0.5	600	12		29.9	14.9	1.69E-10	9.69E-11	20.385
19	7,709	320.6	0.51	50	12		31.1	15.2	1.19E-09	1.30E-09	21.205
20	7,781	320.8	0.5	600	12		31.2	15.6	2.02E-10	1.16E-10	21.258
21	7,877	320.5	0.51	50	12		31.8	15.6	1.43E-09	1.42E-09	21.653
22	7,950	321.1	0.5	600	12		32.0	16.0	2.15E-10	1.29E-10	21.710
23	8,048	320.9	0.5	50	12		32.6	16.3	1.41E-09	1.66E-09	22.113
24	8,117	320.6	0.5	600	12		32.8	16.4	2.29E-10	1.42E-10	22.172
25	8,285	321.1	0.51	50	12		34.1	16.7	1.42E-09	1.90E-09	22.871
26	8,383	320.9	0.5	600	12		34.2	17.1	2.10E-10	1.68E-10	22.944
27	8,813	320.9	0.5	600	12	7,200	34.6	17.3	2.17E-11	1.36E-11	22.976
28	9,320	321.2	1	0	0		34.5	0.0	1.20E-12	-	22.979
29	9,325	321.2	0.5	50	12		33.2	16.6	7.93E-10	1.80E-09	22.992
30	9,341	320.7	0.5	600	12		33.4	16.7	1.92E-10	1.53E-10	23.001
31	9,394	320.8	0.5	50	12		33.6	16.8	1.21E-09	1.88E-09	23.191
32	9,461	320.6	0.5	600	12		33.8	16.9	1.93E-10	1.60E-10	23.232
33	9,510	320.6	0.5	50	12		34.0	17.0	1.27E-09	1.98E-09	23.419
34	9,653	321.5	0.5	600	12		34.5	17.2	1.82E-10	1.76E-10	23.535
35	9,726	321.4	0.5	50	12		34.9	17.4	1.44E-09	2.21E-09	23.832

Table 8 (cont.)

Test Period	Test Time, h	Temp., °C	Load Ratio R	Rise Time, s	Down Time, s	Hold Time, s	K_{max}, MPa·m$^{1/2}$	ΔK, MPa·m$^{1/2}$	CGR_{env}, m/s	Estimated CGR_{air}, m/s	Crack Length, mm
36	9,848	321.2	0.5	600	12		35.1	17.6	1.96E-10	1.89E-10	23.917
37	9,965	321.4	0.5	600	12	7,200	35.4	17.7	2.47E-11	1.50E-11	23.924
38	10,703	321.1	1	0	0		35.3	0.0	3.63E-12	-	23.928
39	11,063	321.7	0.5	50	12		40.6	20.3	2.07E-09	4.13E-09	25.785
40	11,231	320.1	0.5	600	12		41.2	20.6	4.16E-10	3.61E-10	26.041
41	12.387	320.5	0.5	600	12	7,200	41.7	20.8	4.31E-11	2.91E-11	26.216
42	13,361	320.1	1.0	0	0		41.7	0.0	2.48E-12	-	26.217

[a]Simulated PWR water with 2 ppm Li, 1100 ppm B, and 2 ppm. DO<10 ppb. Conductivity was 21±3 μS/cm, and pH 6.4.

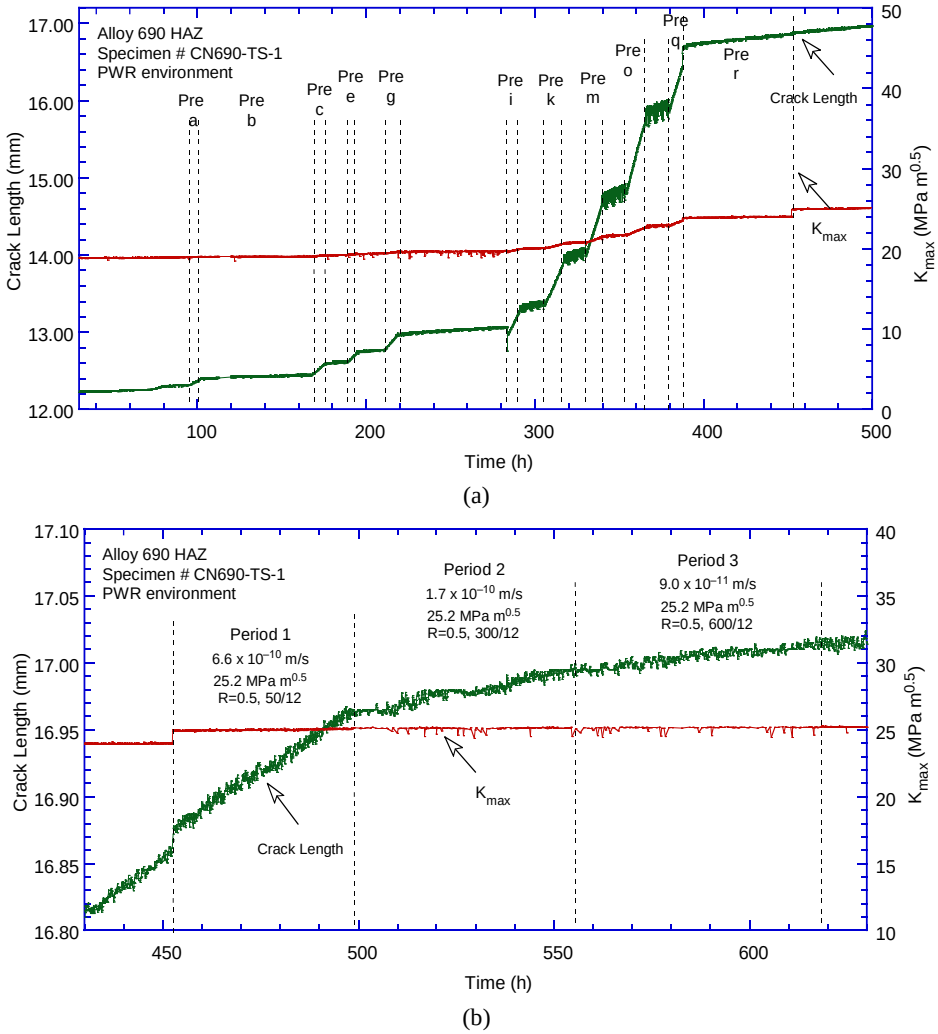

Figure 21 Crack–length–vs.–time for Alloy 152 specimen CN690-TS-1 in simulated PWR environment during test periods (a) precracking, (b) 1-3, (c) 4, (d) 5-7, (e) 8-10, (f) 11-12, (g) 13-19, (h) 21-26, (i) 27-28, (j) 29-37, (k)38, (l) 39-40, (m) 41, and (n) 42.

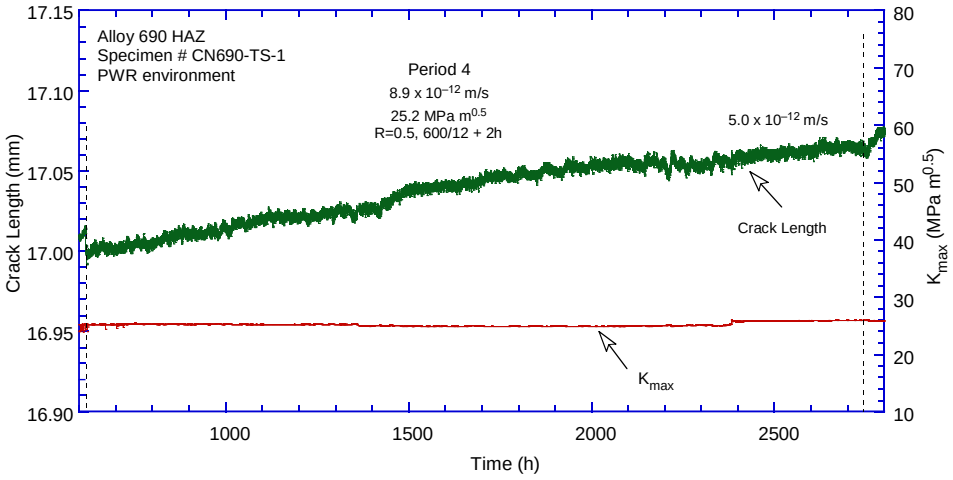

(c)

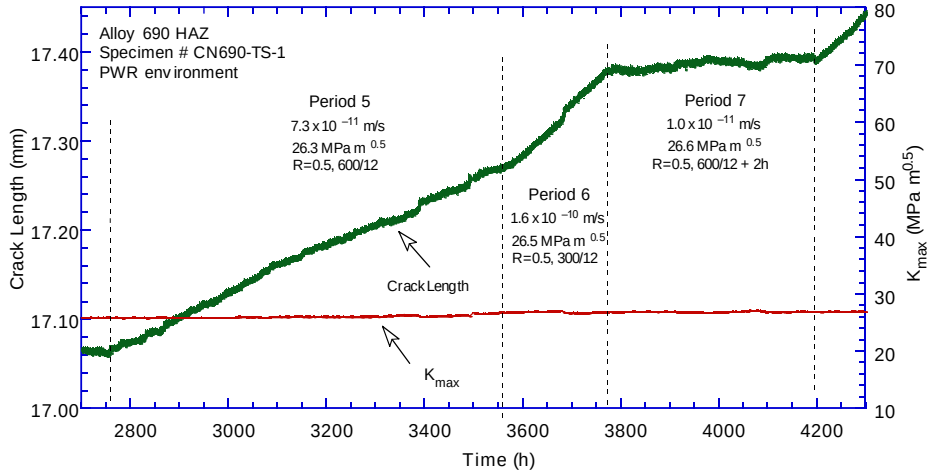

(d)

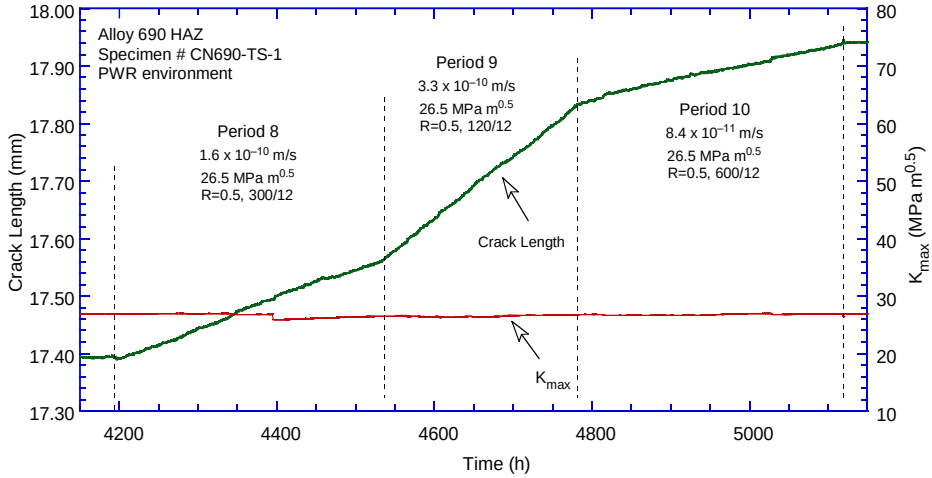

(e)

Figure 21 (cont.)

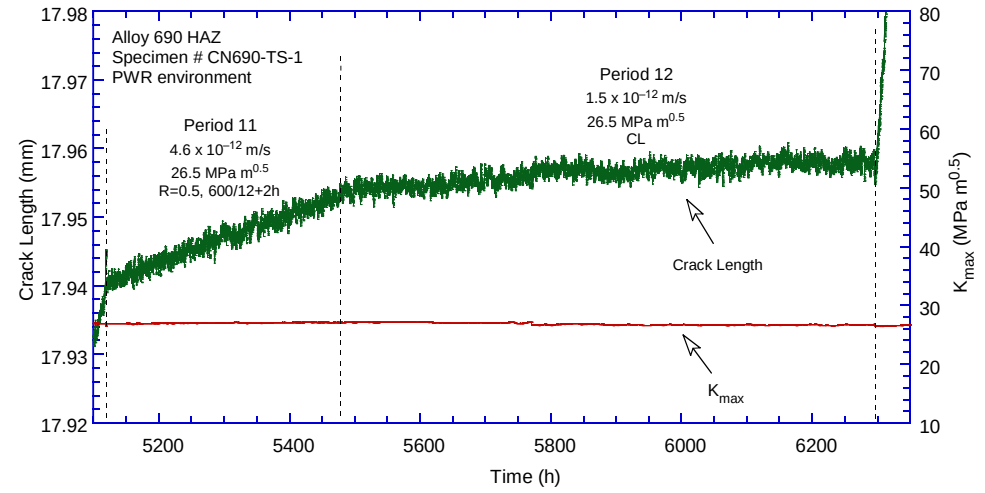

(f)

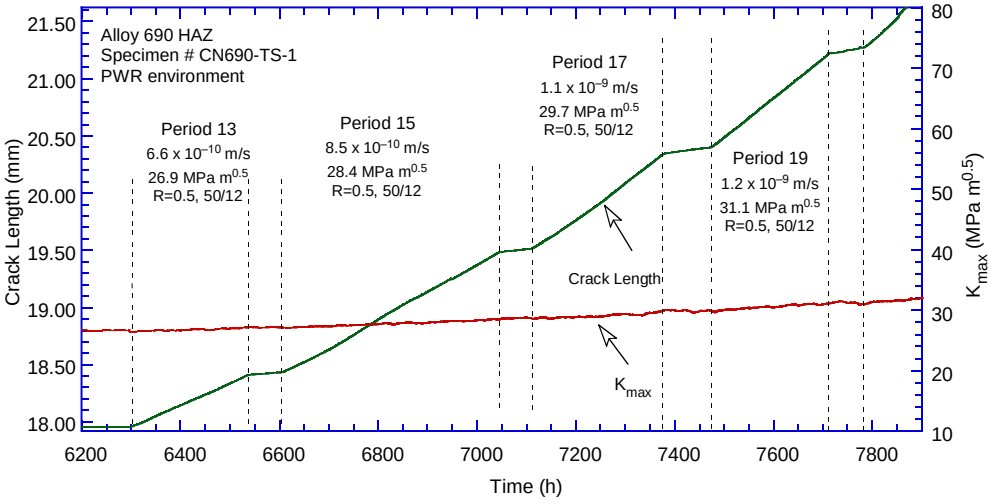

(g)

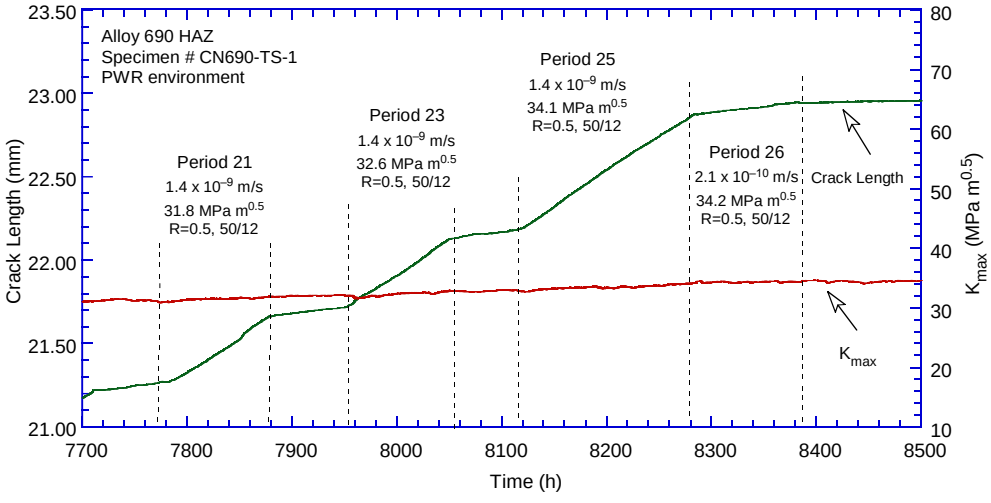

(h)

Figure 21 (cont.)

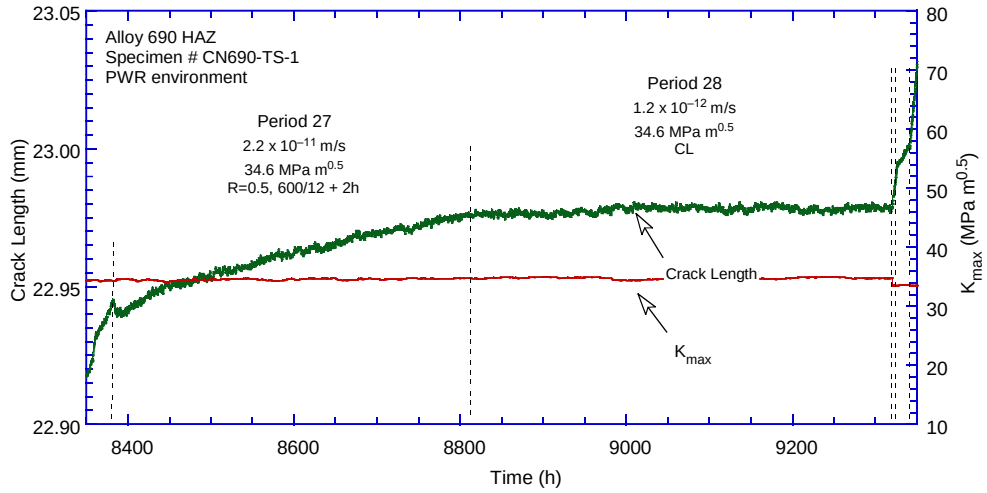

(i)

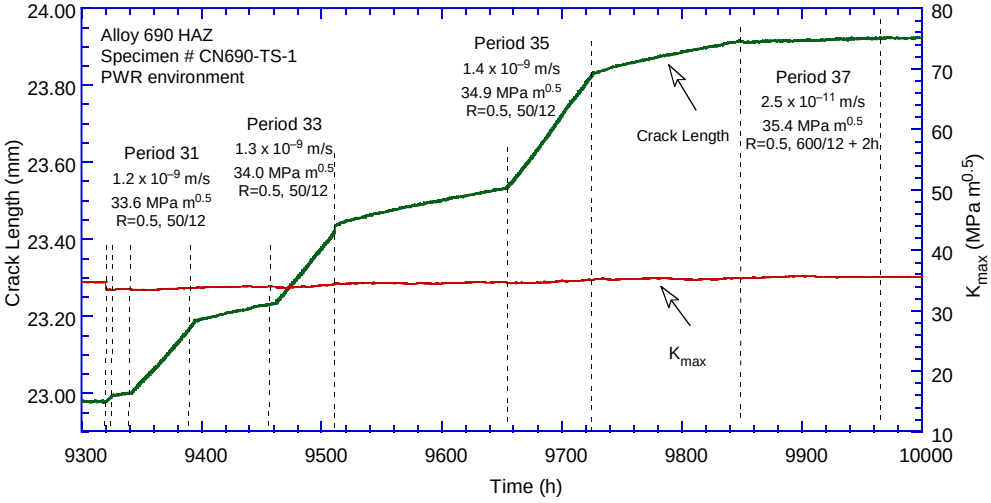

(j)

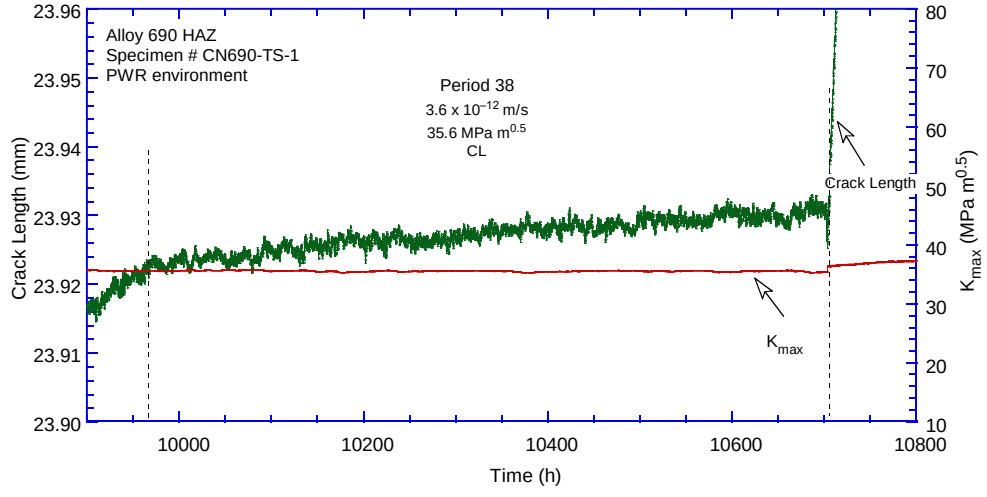

(k)

Figure 21 (cont.)

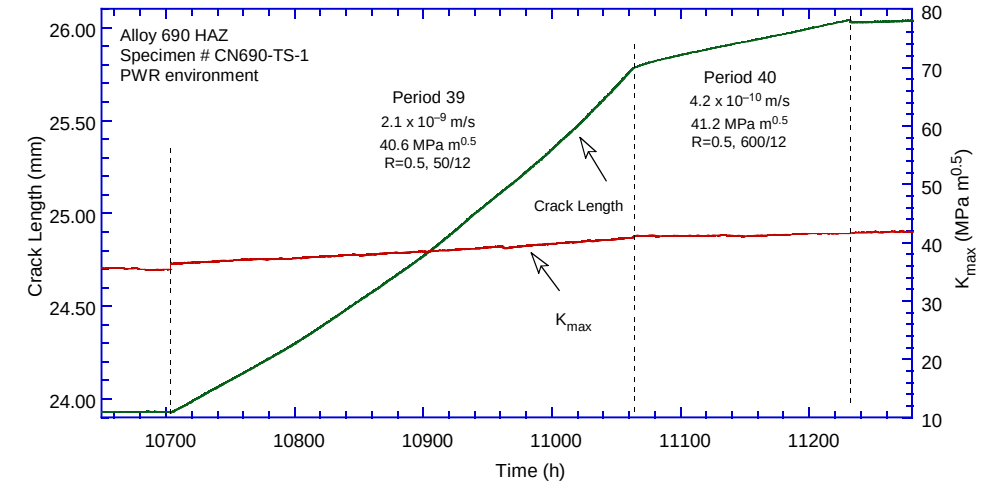

(l)

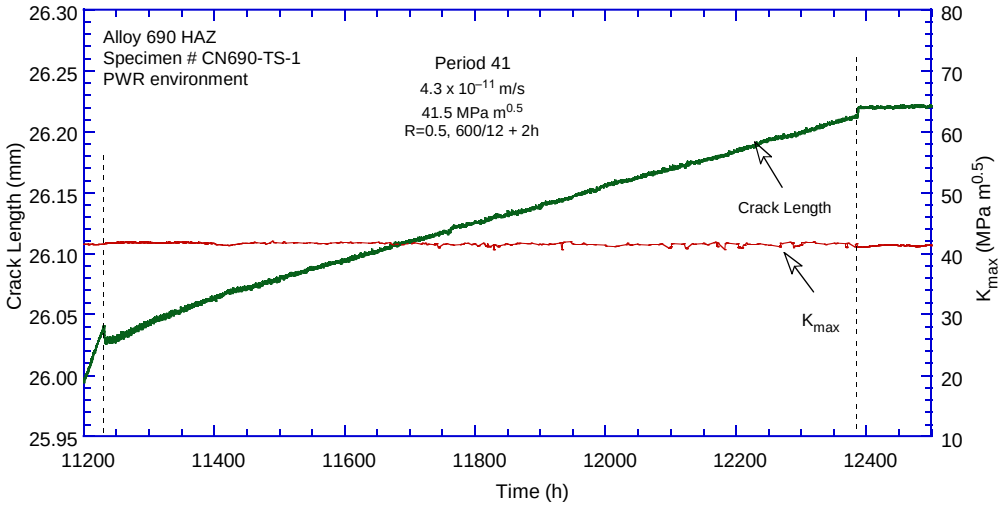

(m)

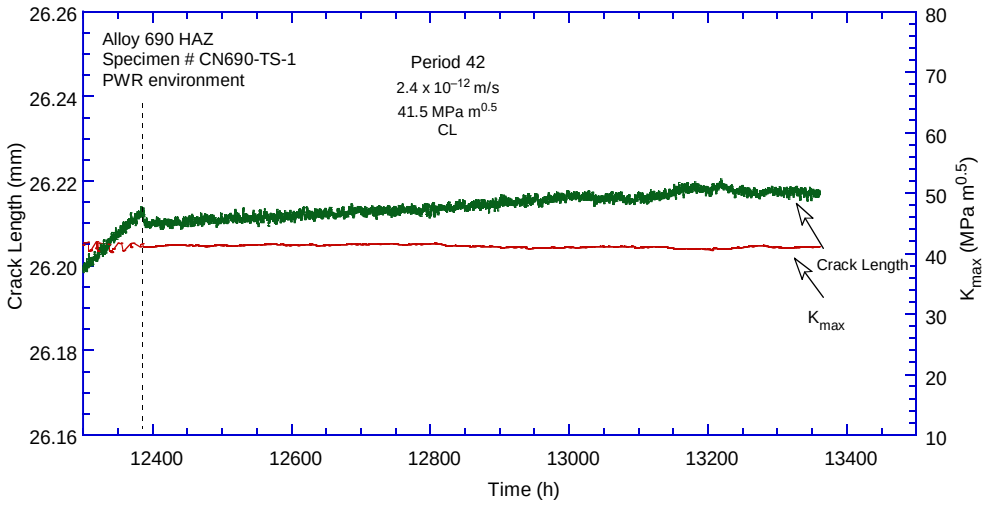

(n)

Figure 21 (cont.)

After the test, the side surfaces were ground to remove the side grooves, polished and etched, Figure 22. Both images show that the distance from the specimen notch to the weld interface was underestimated during the specimen alignment phase by using a "straight line" approach to describe the interface. This is most evident on side 1 (Figure 22a) where the crack intersects one weld lobe fairly early in the test. The blue arrows indicate the intersection with the weld, and the red arrows mark the end of the test. The crack intersects the interface after 3.4 mm on Side 1 and 4.4mm on Side 2; the full extent of the crack is on average 13.4 mm, largely in line with the DC potential measurement of 13.99 mm. After the intersection with the weld, the crack departs from the original propagation direction by approx. 20°, and extends well-outside the specimen side grooves. On the Side 2 picture (Figure 22b) a weld flaw from which additional cracks seem to emanate is also visible. In order to further examine this area, an approx. 2 mm-thick slice was cut from this side of the specimen prior to breaking it open. This slice is available and will be used to provide a reference for the non-aged weld in that region.

After the 2 mm-thick cross section was cut from the specimen, the specimen was broken open to expose the fracture surface, Figure 23. The crack intersects the weld interface after 3.95 mm and grows for a total of 14.16 mm, in excellent agreement (1%) with the DC potential measurement. No DC potential data corrections were necessary. Figure 24 shows the fracture surface observed at the end of the test. The fracture shows a high degree of IG/interdendritic engagement (70%).

In summary, the test on specimen CN690-TS-1 – intended to be a test on Alloy 690 HAZ, ended up being a test of the unaged Alloy 152 weld. The specimen was aligned at a narrow angle with respect to the fusing line, but the crack hit the weld lobes earlier than anticipated. After hitting the weld interface, the crack started propagating at an approximately 20° angle with respect to the original direction. The SCC CGRs were smaller than those measured in the middle of the weld (Figure 4), and in the final test period, it was verified that the test has resulted in a large IG engagement in the Alloy 152 weld.

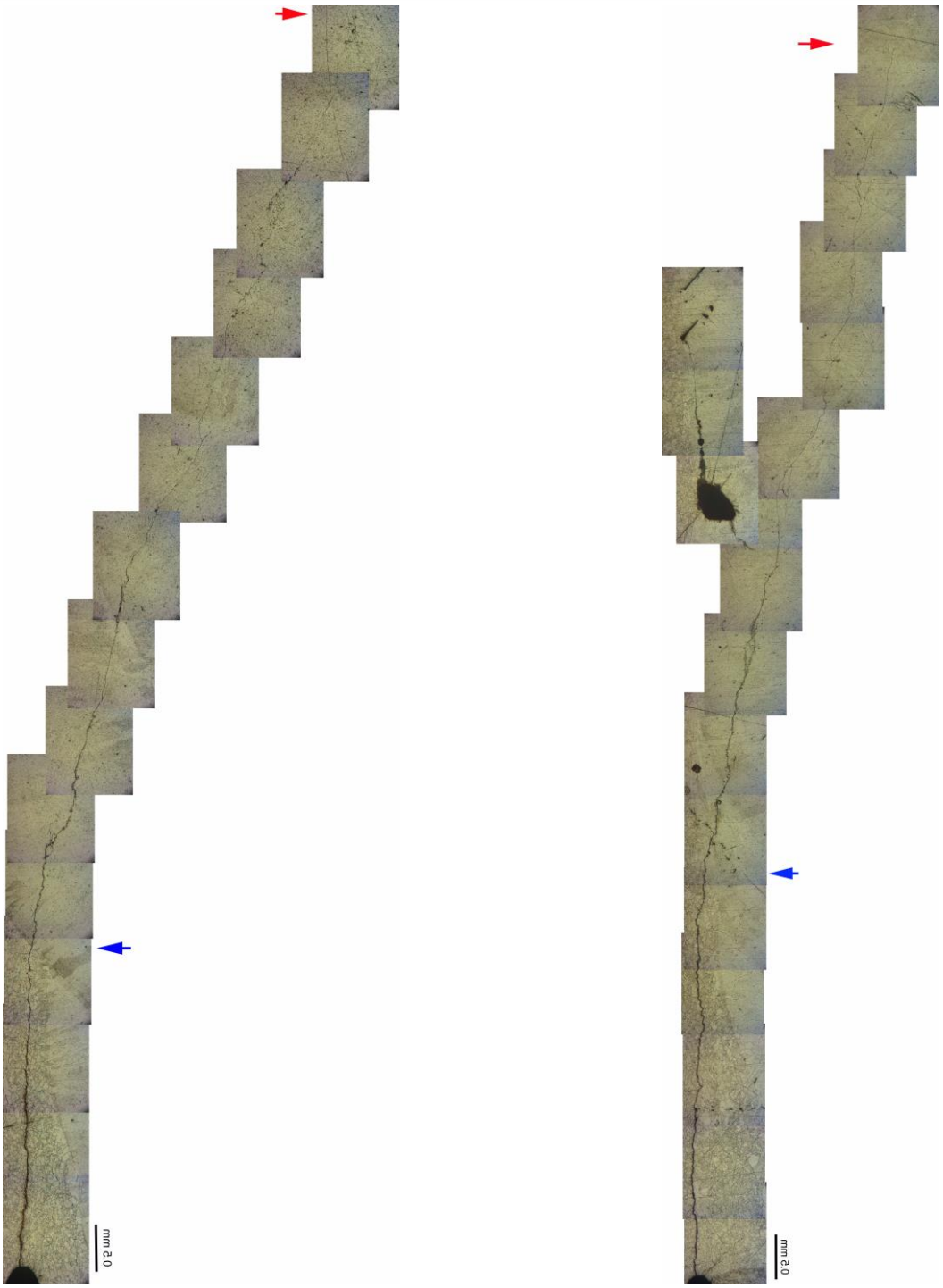

(a) (b)

Figure 22 **Side surfaces of specimen CN690-TS-1: (a) side 1, and (b) side 2. Blue arrows indicate the locations where the crack intersected the Alloy 152 weld, and the red arrows indicate the end of the test. Crack advance is from bottom to top.**

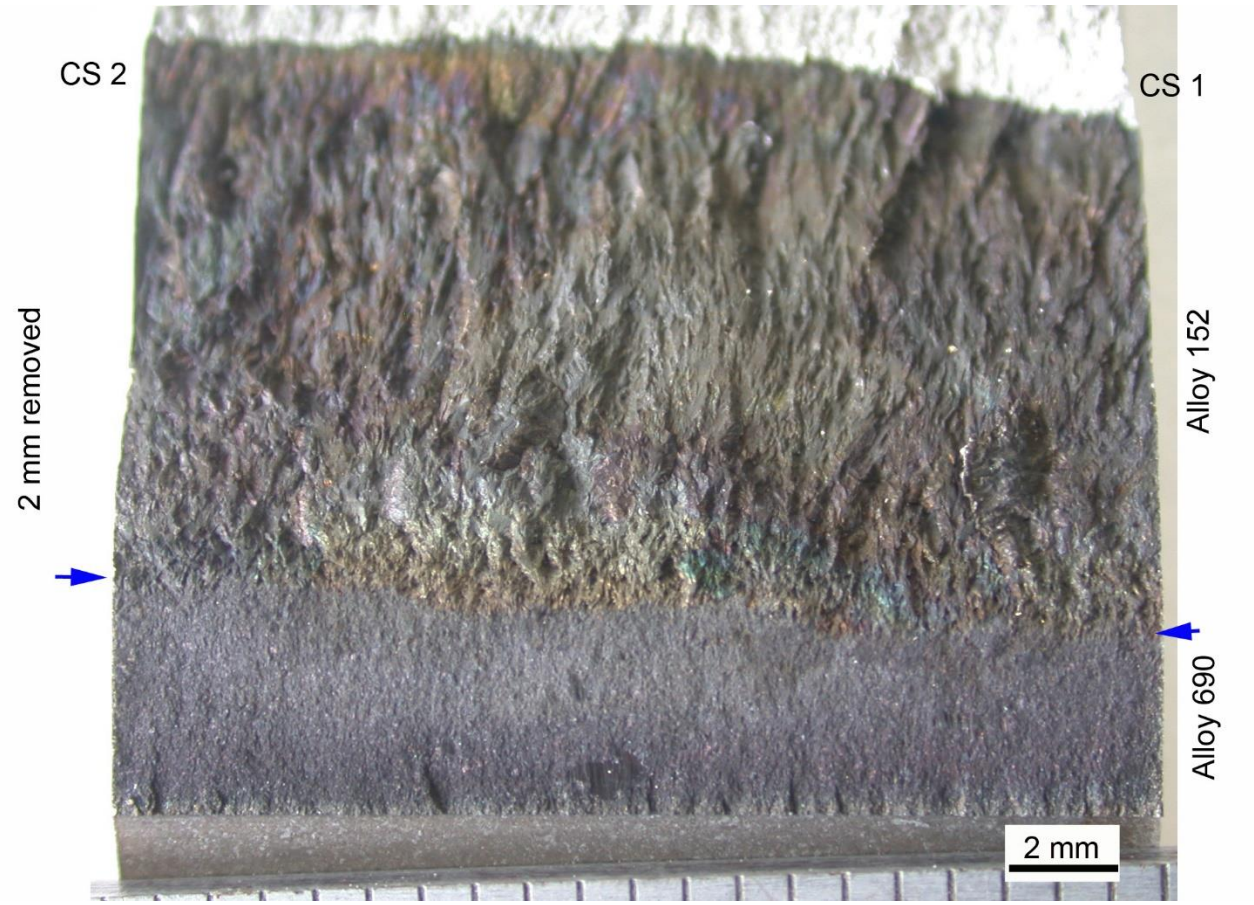

Figure 23 **Fracture surface of Specimen CN690-TS-1. The blue arrows indicate the transition from Alloy 690 to the Alloy 152 weld.**

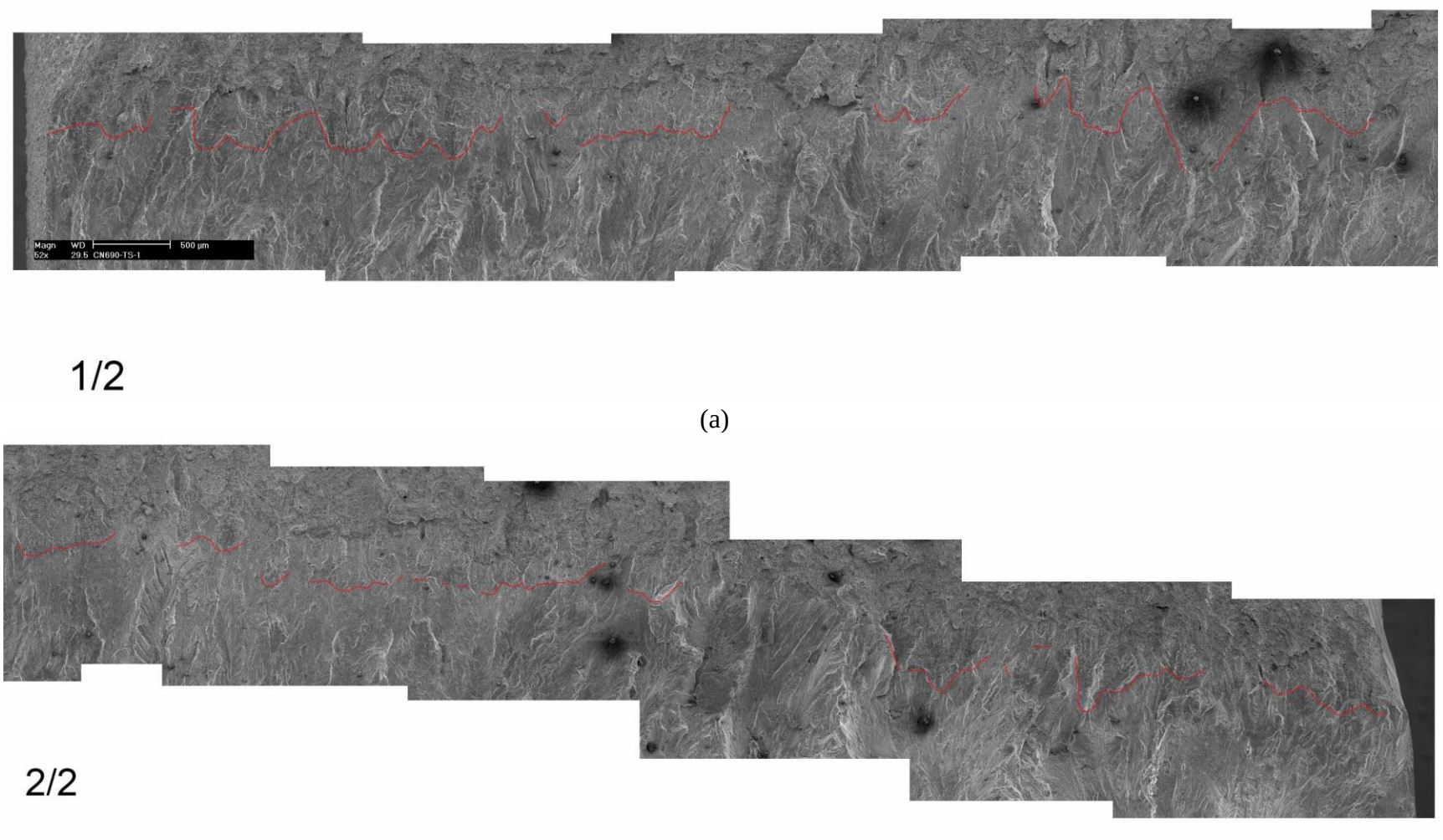

Figure 24 **Fracture surface of Specimen CN690-TS-1 at the end of the test: (a) first half, and (b) second half. The red line indicated almost continuous IG fracture at the end of the test. Crack advance is from bottom to top.**

4 Discussion

This section provides summary of the aging effects in Alloy 152 and discusses the potential implications on performance. The testing results of aged alloys are discussed in the framework provided by the well-established fatigue and corrosion fatigue behavior for these alloys, as well as the industry-proposed disposition curves for crack growth.

4.1 Effects of aging on microstructure of Alloy 152

4.1.1 Long range ordering (LRO) in aged Alloy 152

Weldments – including weld butter layers – add several layers of complexity when compared to the base alloys: grain morphology, retained internal stress, segregation, precipitates, etc. All those factors may evolve with service time, as well as affect the formation of ordered phases such as LRO, for example, by altering the local diffusivity. Moreover, both microstructure and ordered phases can affect SCC.

The three Alloy 152 heats WC04F6, 720129, and 146444 aged to 60 years of service equivalent did not show ordering. While LRO and its effect on SCC response is one of the main questions that this research is attempting to answer, it is important to keep in mind that the microstructural effects of thermal aging have been studied extensively in the past, leading to a comprehensive understanding of thermally-induced Cr carbide precipitation along grain boundaries [25], further resulting into an overall increase in hardness. From an SCC susceptibility standpoint, Cr carbide precipitation depletes Cr from solution, and thus could potentially decrease resistance to SCC. In essence, an increase in hardness, whether due to LRO formation or Cr-carbide precipitation, or both, can potentially have a negative effect on the SCC resistance, and hence needs to be investigated experimentally. The SCC CGR test undertaken in this program and presented in this report addresses that need.

The location of analysis within a weld is expected to play a role and potentially affect local diffusivity and outcomes of analysis just described. Hence, it is anticipated, that further characterization – such as hardness mapping – will be conducted with the purpose of identifying potentially vulnerable regions.

In order to address these concerns, future microstructural characterization will likely include hardness/nanohardness mapping, chemistry mapping and targeted XRD analysis.

4.2 Effects of aging on crack growth response of Alloy 152

4.2.1 Cyclic response of aged Alloy 152

Figure 25 presents the cyclic CGR data obtained on Alloy 152 heat WC04F6 in the as-received and aged conditions. In the figure, the cyclic CGRs measured in the environment are plotted vs. the CGRs predicted in air under the same loading conditions for Ni-based weldments. In this representation, the environmental enhancement, i.e., the departure from the "1:1 diagonal" can be easily visualized. Correlations describing cyclic CGRs in air and LWR environments have been established by ANL for Alloy 600, 690, Ni-base weldments as well as SSs [26-30]. For comparison, the expected cyclic CGR curve for Alloy 182 weld was also included. Figure 25 shows that, as expected, the cyclic CGRs in the mechanical fatigue regime (10^{-8}-10^{-7} m/s) are exactly as expected, and that is true for both aged and un-aged specimens. Likewise, in the corrosion fatigue regime (10^{-11}-10^{-9} m/s), there is no difference

between the aged and non-aged specimens. Also, unsurprisingly, at the lower end of the spectrum, the environmental enhancement of all Alloy 152 specimens is lower than the Alloy 182 curve – likely an effect of the higher Cr content.

In summary, the fatigue and corrosion fatigue CGR response of the Alloy 152 heat WC04F6 specimen aged to 60-year service equivalents is similar to that of the un-aged condition.

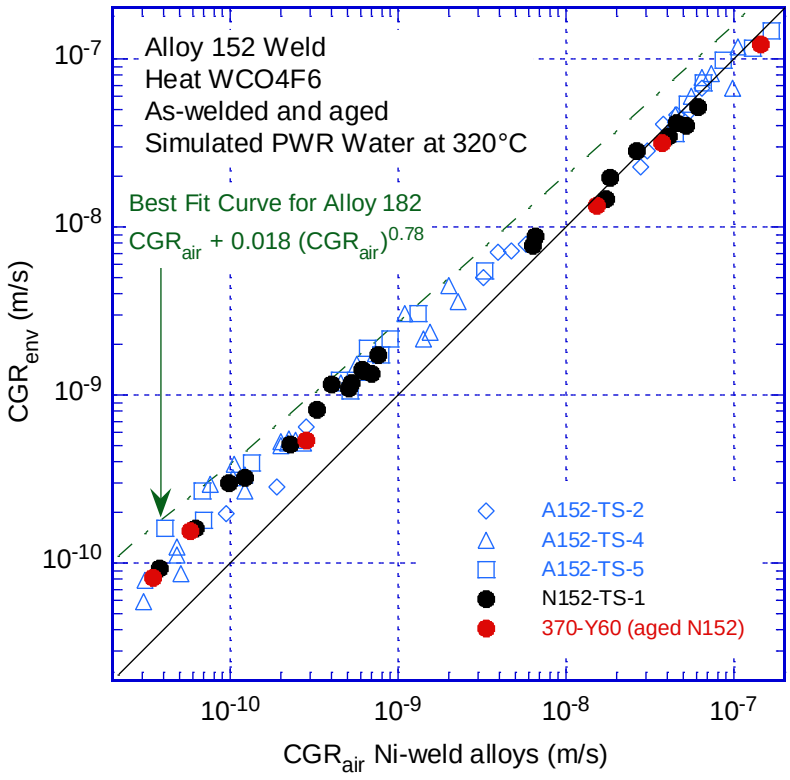

Figure 25 Cyclic CGRs measured in the environment vs. CGRs predicted in air under the same loading conditions for Alloy 152 weld heat WC04F6 in the as-received and aged conditions..

4.2.2 SCC response of aged Alloy 152

Figure 26 presents the SCC CGR data for the Alloy 152 heat WC04F6 in the non-aged [15, 17] and aged conditions vs. stress intensity factor, K. For context, the proposed disposition curves for Alloys 182 [1] and 52/152 [2] are included in the figures. The SCC CGR data for the aged specimen 370-Y60 N152 shown in Figure 26b seems to be similar to the data obtained on non-aged conditions in the middle of the weld (Figure 26a). However, when data from the same region of the weld in compared, Figure 26b, aging to 60-year service equivalent appears to have a negative effect on the SCC resistance of this Alloy 152 heat. The EPRI MRP-386 [2] proposed disposition curve does not seem to bound any of the SCC CGR for this weld heat, in either non-aged or aged condition.

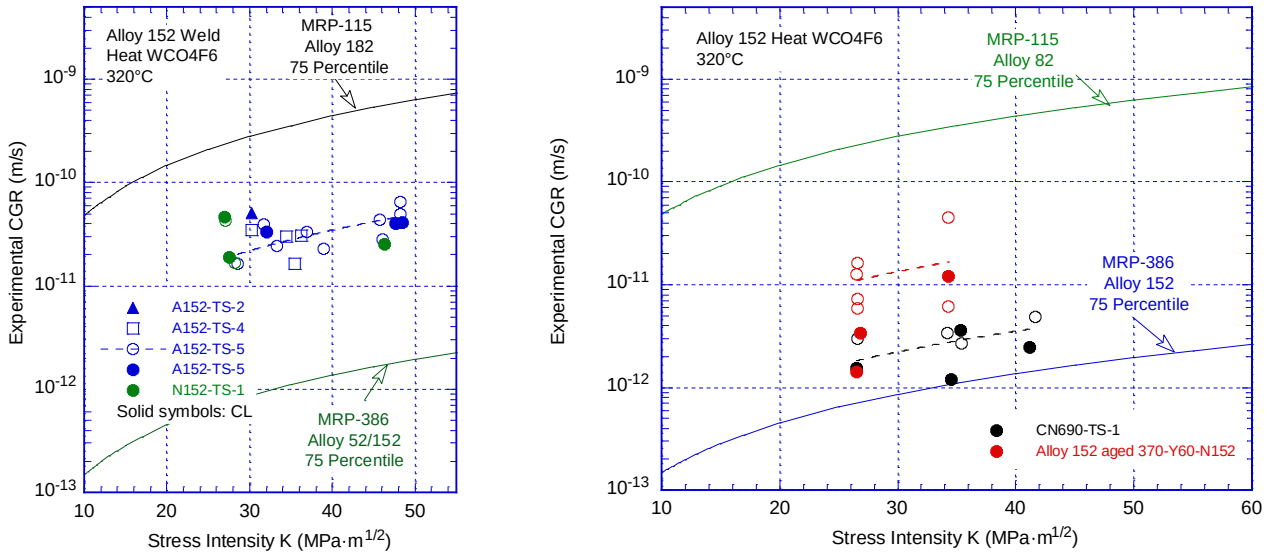

Figure 26 **SCC CGRs for Alloy 152 weld heat WC04F6 in the (a) as- received [15, 17], and (b) as-received and aged conditions. Solid symbols represent SCC CGRs measured under constant load (CL) and open symbols represent SCC CGRs measured under periodic partial unloading (PPU) conditions. The proposed disposition curves for Alloys 182 [1] and 52/152 [2] are included.**

5 Conclusions

The need for an assessment of the long term aging effects on performance in Alloy 690 and associated weldments was identified as a research gap in the Light Water Reactor Sustainability (LWRS) stakeholders report for 2020 [9], being recognized as such by both industry [2, 10] and regulators [11]. The research undertaken in this program is beginning to address that gap. Specifically, the work focused on the microstructural evolution and the SCC response of Alloy 152 under accelerated thermal aging and conditions. The materials studied involved three heats of Alloy 152, aged at three different temperatures (370°C, 400°C and 450°C) for up to 75,000h. The conclusions of this research are as follows:

- For three heats of Alloy 152 weld, aging to 60 year equivalent service did not find evidence of LRO.
- Testing in a primary water environment of an Alloy 152 heat WC04F6 specimens aged at 370°C to a 60-year service equivalent revealed a fatigue and corrosion fatigue crack growth responses similar to those measured on the un-aged alloy.
- The SCC CGR data for the aged specimen seems to be similar to the data obtained on non-aged conditions in the middle of the weld. However, when data from the same region of the weld are compared, aging to 60-year service equivalent appears to have a negative effect on the SCC resistance of this Alloy 152 heat. Further investigations are needed to understand and substantiate the effect. The EPRI MRP-386 [2] proposed disposition curve does not seem to bound any of the SCC CGR for this weld heat, in either non-aged or aged condition.

References

1. Materials Reliability Program: Crack Growth Rates for Evaluating Primary Water Stress Corrosion Cracking (PWSCC) of Alloy 82, 182, and 132 Welds (MRP-115), EPRI, Palo Alto, CA: 2004. 1006696.
2. Electric Power Research Institute, "Recommended Factors of Improvement for Evaluating Primary Water Stress Corrosion Cracking (PWSCC) Growth Rates of Thick-Wall Alloy 690 Materials and Alloy 52, 152, and Variants Welds (MRP-386)," Palo Alto, CA, 2017: 3002010756.
3. Young, G.A., Morton, D.S., Lewis, N. Morris, R., Pyle, J., Barnard, L., Najafabadi, R., Effect of Long Range Order on the Stress Corrosion Susceptibility of a Nickel-33 at% Chromium Alloy, Corrosion 72 2016 1433.
4. Marucco, A., Atomic Ordering in the Ni-Cr-Fe system, Mat. Sci. and Eng. A189 (1994) 267.
5. F. Delabrouille, D. Renaud, F. Vaillant, J. Massoud, Long range ordering of Alloy 690, in: 14th. Int. Conf. On Environmental Degradation of Materials in Nuclear Power Systems, 2009, pp. 888-894.
6. Brimbal, D., Joly, P., Benhamou, C., Thermal aging of Ni-Cr and Ni-Cr-Fe alloys to determine the potential for long-range ordering of Alloy 690 at PWR relevant temperatures, EPRI PWSCC Research Collaboration Meeting 2019, Tampa, Florida, December 4th, 2019.
7. Houtilainen, C., Ehrnstén, U., Ahonen, M., Hänninen, H., Effect of Thermal Aging on Microstructure and Hardness of Industrial Heats of Alloy 690, 19th. Int. Conf. On Environmental Degradation of Materials in Nuclear Power Systems, 2019.
8. Song, M., Yang, Y., Wang, M., Kuang, W., Lear, C.L., Was, G.S., Probing long-range ordering in nickel-base alloys with proton Irradiation, Acta Materialia 156 (2018) 446-462.
9. Light Water Reactor Sustainability Program Stakeholder Engagement Meeting Summary Report, INL/EXT-19-54520, February, 2020.
10. Burke, M., Coordination of EPRI Issue Programs' Research Activities with LWRS Materials Pathway Projects, LWRS Materials Research Pathway Stakeholder Engagement Meetings, August 18, 2020.
11. Collins, J., and Focht, E., Nickel-Based Alloy Crack Growth Rates, Industry / NRC Materials Programs Technical Information Exchange, August 11, 2021, ML21217A260.
12. Alexandreanu, B., Chen, Y., Zhang, X., and W. Y. Chen, "Effect of Thermal Aging and Irradiation on Microstructure and Crack Growth Response in Alloy 690," ANL/LWRS- 21/1, September 2021.
13. Material Documentation Report for Consumers Power Midland (620-0012-51) and TMI-2 (620-0006-51) Reactor Vessel Lower Head Material, The Babcock & Wilcox Company, BAW-2071, January 1989.
14. Dunn, D., Alexandreanu, B., Toter, W., "Shielded Metal Arc Welding Parameters for Primary Water Stress Corrosion Cracking Test Materials," Technical Letter Report ML13171A113, June 2013.
15. Alexandreanu, B., Y. Yang, Y. Chen, and W. J. Shack, "Stress Corrosion Cracking in Nickel-Base Alloys 690 and 152 Weld in Simulated PWR Environment - 2009," NUREG/CR–7137, ANL–10/36, June 2012.
16. Alexandreanu, B., Chen, Y., Natesan, K., and Shack, "Primary Water Stress Corrosion Cracking of High-Chromium, Nickel-Base Welds Near Dissimilar Metal Weld Interfaces," NUREG/CR–7226, ANL–16/10, January 2018.
17. Alexandreanu, B., Chen, Y., Natesan, K., and Shack, "Primary Water Stress Corrosion Cracking of High-Chromium, Nickel-Base Welds - 2018," NUREG/CR–7276, 2021.

18. Choi, K.J., Kim, J.J, Bong, H.L., Bahn, C.B., Kim, J.H., Effects of thermal aging on microstructures of low alloy steel–Ni basealloy dissimilar metal weld interfaces, Journal of Nuclear Materials 441 (2013) 493-502.
19. Yoo, S.C., Choi, K.J., Bahn, C.B., Kim, S.H., Kim, J.Y., Kim, J.H., Effects of thermal aging on the microstructure of Type-II boundaries in dissimilar metal weld joints, Journal of Nuclear Materials 459 (2015) 5-12.
20. B. Alexandreanu, B. Capell and G.S. Was, Combined Effect of Special Grain Boundaries and Grain Boundary Carbides on IGSCC of Ni-16Cr-9Fe-xC Alloys, *Mat. Sci. and Eng.* A 300 (2001) 94.
21. Gwalani, B., Alam, T., Miller, C., Rojhirunsakool, T., Kim, Y.S., Kim, S.S., Kaufman, M., Ren, Y., and Banerjee, R., (2016). Experimental investigation of the ordering pathway in a Ni-33 at.%Cr alloy. Acta Materialia. 115. 372-384. 10.1016/j.actamat.2016.06.014.
22. American Society for Testing and Materials, "Standard Test Method for Measurement of Fatigue Crack Growth Rates," ASTM E647-08, DOI 10.1520/E0647-08, West Conshohocken, PA, 2008.
23. American Society for Testing and Materials, "Standard Test Method for Determining a Threshold Stress Intensity Factor for Environment-Assisted Cracking of Metallic Materials," ASTM E1681-03, DOI 10.1520/E1681-03R08, West Conshohocken, PA, 2008.
24. Electric Power Research Institute, "PWR Primary Water Chemistry Guidelines," Volume 1, Revision 4, EPRI, Palo Alto, CA, 1999.
25. Angeliu, T.M., and Was, G.S., Behavior of grain boundary chemistry and precipitates upon thermal treatment of controlled purity Alloy 690, Metall. Trans. A 21A, 2097 (1990).
26. Ruther, W. E., W. K. Soppet, and T. F. Kassner, "Corrosion Fatigue of Alloys 600 and 690 in Simulated LWR Environments," NUREG/CR-6383, ANL-95/37, April 1996.
27. Ruther, W. E., W. K. Soppet, T. F. Kassner, and W. J. Shack, "Environmentally Assisted Cracking of Alloys 600 and 690 in Simulated LWR Water," in Environmentally Assisted Cracking in Light Water Reactors, Semiannual Report, January 1998-July 1998, NUREG/CR-4667, Vol. 26, ANL-98/30, pp. 25-32, March 1999.
28. Chopra, O. K., W. K. Soppet, and W. J. Shack, "Effects of Alloy Chemistry, Cold Work, and Water Chemistry on Corrosion Fatigue and Stress Corrosion Cracking of Nickel Alloys and Welds," NUREG/CR-6721, ANL-01/07, April 2001.
29. Alexandreanu, B., O. K. Chopra, and W. J. Shack, "Crack Growth Rates of Nickel Alloys from the Davis-Besse and V. C. Summer Power Plants in a PWR Environment," NUREG/CR–6921, ANL–05/55, November 2006.
30. Alexandreanu, B., O. K. Chopra, and W. J. Shack, "Crack Growth Rates of Nickel Alloy Welds in a PWR Environment," NUREG/CR–6907, ANL–04/3, May 2006.
31. Electric Power Research Institute, "Materials Reliability Program (MRP) Crack Growth Rates for Evaluating Primary Water Stress Corrosion Cracking (PWSCC) of Thick-Wall Alloy 600 Materials (MRP-55)," Revision 1, 1006695, Palo Alto, CA, 2002.

This page intentionally left blank

Nuclear Engineering Division
Argonne National Laboratory
9700 South Cass Avenue, Bldg. 208
Argonne, IL 60439

www.anl.gov